



Article

# Effect of Gold Electronic State on the Catalytic Performance of Nano Gold Catalysts in *n*-Octanol Oxidation

Ekaterina Pakrieva <sup>1,2,\*</sup> , Ekaterina Kolobova <sup>1</sup>, Yulia Kotolevich <sup>3</sup> , Laura Pascual <sup>2</sup>, Sónia A. C. Carabineiro <sup>4</sup> , Andrey N. Kharlanov <sup>5</sup>, Daria Pichugina <sup>5</sup>, Nadezhda Nikitina <sup>5</sup>, Dmitrii German <sup>1</sup>, Trino A. Zepeda Partida <sup>3</sup>, Hugo J. Tiznado Vazquez <sup>3</sup> , Mario H. Farías <sup>3</sup>, Nina Bogdanchikova <sup>3</sup>, Vicente Cortés Corberán <sup>2</sup> and Alexey Pestryakov <sup>1,\*</sup>

<sup>1</sup> Research School of Chemistry & Applied Biomedical Sciences, National Research Tomsk Polytechnic University, Lenin Av. 30, 634050 Tomsk, Russia; ekaterina\_kolobova@mail.ru (E.K.); germandmitry93@gmail.com (D.G.)

<sup>2</sup> Instituto de Catálisis y Petroleoquímica, Consejo Superior de Investigaciones Científicas, Marie Curie 2, 28049 Madrid, Spain; laura.pascual@icp.csic.es (L.P.); vcortes@icp.csic.es (V.C.C.)

<sup>3</sup> Centro de Nanociencias y Nanotecnología, Universidad Nacional Autónoma de México, P.O. Box 14, Ensenada 22800, Mexico; julia.kotolevich@gmail.com (Y.K.); trino@cnyn.unam.mx (T.A.Z.P.); tiznado@cnyn.unam.mx (H.J.T.V.); mario@cnyn.unam.mx (M.H.F.); nina@cnyn.unam.mx (N.B.)

<sup>4</sup> LAQV-REQUIMTE, Department of Chemistry, NOVA School of Science and Technology, Universidade, NOVA de Lisboa, 2829-516 Caparica, Portugal; sonia.carabineiro@fct.unl.pt

<sup>5</sup> Department of Chemistry, Lomonosov Moscow State University, 1-3 Leninskiye Gory, GSP-1, 119991 Moscow, Russia; kharl@kge.msu.ru (A.N.K.); dashapi@mail.ru (D.P.); nnikitina1719@gmail.com (N.N.)

\* Correspondence: epakrieva@mail.ru (E.P.); pestryakov2005@yandex.ru (A.P.)

Received: 31 March 2020; Accepted: 29 April 2020; Published: 2 May 2020



**Abstract:** This study aims to identify the role of the various electronic states of gold in the catalytic behavior of Au/M<sub>x</sub>O<sub>y</sub>/TiO<sub>2</sub> (where M<sub>x</sub>O<sub>y</sub> are Fe<sub>2</sub>O<sub>3</sub> or MgO) for the liquid phase oxidation of *n*-octanol, under mild conditions. For this purpose, Au/M<sub>x</sub>O<sub>y</sub>/TiO<sub>2</sub> catalysts were prepared by deposition-precipitation with urea, varying the gold content (0.5 or 4 wt.%) and pretreatment conditions (H<sub>2</sub> or O<sub>2</sub>), and characterized by low temperature nitrogen adsorption-desorption, X-ray powder diffraction (XRD), energy dispersive spectroscopy (EDX), scanning transmission electron microscopy-high angle annular dark field (STEM HAADF), diffuse reflectance Fourier transform infrared (DRIFT) spectroscopy of CO adsorption, temperature-programmable desorption (TPD) of ammonia and carbon dioxide, and X-ray photoelectron spectroscopy (XPS). Three states of gold were identified on the surface of the catalysts, Au<sup>0</sup>, Au<sup>1+</sup> and Au<sup>3+</sup>, and their ratio determined the catalysts performance. Based on a comparison of catalytic and spectroscopic results, it may be concluded that Au<sup>+</sup> was the active site state, while Au<sup>0</sup> had negative effect, due to a partial blocking of Au<sup>0</sup> by solvent. Au<sup>3+</sup> also inhibited the oxidation process, due to the strong adsorption of the solvent and/or water formed during the reaction. Density functional theory (DFT) simulations confirmed these suggestions. The dependence of selectivity on the ratio of Brønsted acid centers to Brønsted basic centers was revealed.

**Keywords:** gold catalysts; *n*-octanol oxidation; gold active sites; gold electronic state; support modifiers; metal content; pretreatment atmosphere; DFT; solvent adsorption; acid-base centers; selectivity

## 1. Introduction

The selective oxidation of alcohols to valuable carbonyl compounds is one of the most crucial transformations in the chemical industry, for both laboratory and industrial manufacturing [1,2]. Traditionally, numerous oxidizing reagents (including toxic, expensive, stoichiometric oxidants [3,4]), along with the use of harmful solvents and harsh reaction conditions, have been employed to accomplish this transformation. Thus, these methods lead to environmental pollution and economic problems [5–8]. Therefore, there is considerable need for more harmless and sustainable technologies, requiring renewable feedstock, e.g., biomass, as replacement for fossil resources [9]. Therefore, a green process, involving the use of non-toxic and cheap oxygen, in the presence of a heterogeneous catalyst (used as a recyclable solid material in biomass processing), in mild conditions (atmospheric pressure, low temperature and absence of bases and radical initiators) would be of great interest [10–13].

Supported gold catalysts have proved to be efficient in the liquid phase oxidation of alcohols, due to their higher selectivity and better resistance to deactivation, compared to their conventional noble metal counterparts [14–17]. However, the effect of a number of parameters, such as gold content, particle size of gold, the preparation method, gold electronic state, influence of support modifiers, redox pretreatment, etc., have not been investigated in detail.

Notably, *n*-octanol belongs to the group of low fatty alcohols, whose physical properties impose constraints to the implementation of green chemistry approaches. One of the demanded oxidation product of *n*-octanol is octanal or caprylic aldehyde, which occurs naturally in citrus oils and could be used commercially as a component in perfumes and in flavor production for the food industry [18]. Compounds of octanoic acid, another *n*-octanol oxidation product, are found naturally in the milk of various mammals, and as a minor constituent of coconut and palm kernel oils [19]. Octanoic acid, also known as caprylic acid, has wide applications. In addition to the commercial production of ester (octyl octanoate) for perfumery, as flavor and fragrance agents, and in the manufacture of dyes, octanoic acid can be used as disinfectant [20] in commercial food handling and health care facilities. In addition, it is currently being investigated as a treatment for voice tremor [21,22] and taken as a dietary supplement [23].

Moreover, *n*-octanol is often used for comparative studies of catalytic activity in oxidation of alcohols, as a convenient model of primary alcohols of long chain. However, among them, there are very few studies where mild conditions have been applied for the efficient and selective liquid phase oxidation of *n*-octanol using gold supported catalysts; they are briefly summarized in Table 1.

Li et al. [24] studied silica-supported Au–Cu and Au–Ag alloy nanoparticles (NPs), for the aerobic oxidation of alcohols. For comparison, they also investigated the corresponding monometallic catalysts in octanol oxidation. With a large catalyst load, 6 wt.% Au/SiO<sub>2</sub> (alcohol/Au ratio, R = 8), they achieved 40% conversion of *n*-octanol in 4 h, with 17% aldehyde selectivity. Unfortunately, no information of other products nor of electronic state of gold was provided.

Su et al. [25] suggested that the high dispersion of Au NPs and the electron donation effects of aryl rings to the Au NPs within the large cages of the MIL-101 support are the main reasons for the observed high activities of the Au/MIL-101 catalyst in the aerobic oxidation of alcohols, including *n*-octanol, under base-free conditions.

Liu et al. [26] showed that Au/ $\gamma$ -Ga<sub>2</sub>O<sub>3</sub> was effective for the oxidation of several alcohols. In particular, 45% octanol conversion was obtained after 2.5 h with 99% aldehyde selectivity, using a low alcohol/Au ratio (R = 10). Nevertheless, the high catalytic performance exhibited was attributed to the significantly enhanced dehydrogenation capabilities, due to a strong interaction between Au NPs and the  $\gamma$ -Ga<sub>2</sub>O<sub>3</sub> support, which was attributed to the presence of gold species detected by XPS with binding energy (BE) 83.1–83.4 eV.

Haider et al. [27] described the oxidation of various types of alcohols over 1 wt.% Au/Cu<sub>a</sub>Mg<sub>b</sub>Al<sub>c</sub>O<sub>x</sub> catalysts. In the case of *n*-octanol oxidation, 34% octanal yield was obtained at 90 °C after 3 h (Table 1). Ex situ XANES of the fresh and spent catalysts revealed that a significant fraction of the deposited gold existed as charged species (Au<sup>+</sup>).

In a recent paper [28], MgO, ZnO and Nb<sub>2</sub>O<sub>5</sub>, representative of three different types of oxides (basic, amphoteric and acidic, respectively), were used as supports for Au NPs. It was found that the catalytic activity is influenced by the electron mobility between the Au NPs and the support, which depends on the intermediate electronegativity of the support. However, besides the predominant (Au<sup>0</sup>)<sup>δ-</sup> species in some active dried catalysts (2 wt.% Au-MgO-D and 2 wt.% Au-ZnO-D), cationic gold (Au<sup>+</sup>) was also present. Selectivity in *n*-octanol oxidation, preferably towards ester formation in the case of the most active catalyst, was influenced by redox properties of the gold species, acid-base properties of the supports and catalyst pretreatment.

Our group widely investigated titania supported Au NPs with different modifiers, gold loading and treatments in *n*-octanol oxidation [29–33] (Table 1). It was found that monovalent gold ions are presumed to be the active sites in Au/M<sub>x</sub>O<sub>y</sub>/TiO<sub>2</sub> (M = La or Ce) [31–33]. The concentration, strength and stability of these sites are determined by the gold content, the nature of the support and modifier, and the pretreatment atmosphere.

**Table 1.** Catalytic oxidation of *n*-octanol using gold catalysts under mild conditions (1 atm, 80 °C).

Catalyst	Au Content, wt. %	Oxidant	Solvent	Reaction time, h	R <sup>c</sup>	Conv., %	Selectivity, %			Ref.
							Aldehyde	Acid	Ester	
Au/SiO <sub>2</sub>	6	O <sub>2</sub>	toluene	4	8	40	17			[24]
Au/Ga <sub>3</sub> Al <sub>3</sub> O <sub>9</sub>	1	O <sub>2</sub>	toluene	3	67	23	99			[25]
Au/MIL-101 <sup>a</sup>	0.5	O <sub>2</sub>	toluene	3	67	38	99			[25]
Au/γ-Ga <sub>2</sub> O <sub>3</sub>	2.5	O <sub>2</sub>	Mes. <sup>d</sup>	2.5	10	45	99			[26]
Au/Cu <sub>a</sub> Mg <sub>b</sub> Al <sub>c</sub> O <sub>x</sub>	1	O <sub>2</sub>	Mes.	3	95	34 <sup>e</sup>	98			[27]
Au-Nb <sub>2</sub> O <sub>5</sub> -D <sup>b</sup>	2	O <sub>2</sub>	<i>n</i> -heptane	6	100	5	58	0	42	[28]
Au-Nb <sub>2</sub> O <sub>5</sub> -H <sup>b</sup>	2	O <sub>2</sub>	<i>n</i> -heptane	6	100	6	45	0	55	[28]
Au-ZnO-D	2	O <sub>2</sub>	<i>n</i> -heptane	6	100	45	18	0	82	[28]
Au-ZnO-H	2	O <sub>2</sub>	<i>n</i> -heptane	6	100	38	20	0	80	[28]
Au-MgO-D	2	O <sub>2</sub>	<i>n</i> -heptane	6	100	65	15	10	75	[28]
Au-MgO-H	2	O <sub>2</sub>	<i>n</i> -heptane	6	100	27	35	15	50	[28]
Au/TiO <sub>2</sub> -pH <sub>2</sub>	4	O <sub>2</sub>	<i>n</i> -heptane	6	100	11	81	3	16	[29]
Au/CeO <sub>2</sub> /TiO <sub>2</sub> -pH <sub>2</sub>	4	O <sub>2</sub>	<i>n</i> -heptane	6	100	23	66	2	32	[29]
Au/La <sub>2</sub> O <sub>3</sub> /TiO <sub>2</sub> -pH <sub>2</sub>	4	O <sub>2</sub>	<i>n</i> -heptane	6	100	40	36	0	64	[29]
Au/Fe <sub>2</sub> O <sub>3</sub> /TiO <sub>2</sub> -pH <sub>2</sub>	4	O <sub>2</sub>	<i>n</i> -heptane	6	100	15	58	0	42	[30]
Au/MgO/TiO <sub>2</sub> -pH <sub>2</sub>	4	O <sub>2</sub>	<i>n</i> -heptane	6	100	20	67	2	31	[30]
Au/TiO <sub>2</sub> -pO <sub>2</sub>	0.5	O <sub>2</sub>	<i>n</i> -heptane	6	100	17	28	52	20	[32]
Au/Fe <sub>2</sub> O <sub>3</sub> /TiO <sub>2</sub> -pO <sub>2</sub>	0.5	O <sub>2</sub>	<i>n</i> -heptane	6	100	41	36	21	43	This
Au/MgO/TiO <sub>2</sub> -pO <sub>2</sub>	0.5	O <sub>2</sub>	<i>n</i> -heptane	6	100	43	38	20	42	work
Au/CeO <sub>2</sub> /TiO <sub>2</sub> -pO <sub>2</sub>	0.5	O <sub>2</sub>	<i>n</i> -heptane	6	100	30	27	43	30	[32]
Au/La <sub>2</sub> O <sub>3</sub> /TiO <sub>2</sub> -pO <sub>2</sub>	0.5	O <sub>2</sub>	<i>n</i> -heptane	6	100	63	26	11	63	[32]
Au/TiO <sub>2</sub> -pO <sub>2</sub>	0.5	TBHP <sup>f</sup>	-	6	5000	27	0	80	20	[33]
Au/CeO <sub>2</sub> /TiO <sub>2</sub> -pO <sub>2</sub>	0.5	TBHP	-	6	5000	30	0	80	20	[33]
Au/La <sub>2</sub> O <sub>3</sub> /TiO <sub>2</sub> -pO <sub>2</sub>	0.5	TBHP	-	6	5000	58	0	80	20	[33]

<sup>a</sup> MIL-101: zeolite-type metal-organic framework; <sup>b</sup> D, dried; H, after thermal reductive treatment; <sup>c</sup> R: alcohol/Au ratio (mol/mol); <sup>d</sup> mes.: mesitylene at 90 °C; <sup>e</sup> Instead of conversion, data on yield of aldehyde is given; <sup>f</sup> TBHP: *tert*-butyl hydroperoxide.

Modification and treatment in a hydrogen atmosphere of 4 wt.% Au/M<sub>x</sub>O<sub>y</sub>/TiO<sub>2</sub> catalysts, where M<sub>x</sub>O<sub>y</sub> = Fe<sub>2</sub>O<sub>3</sub> or MgO modifiers, lead to the enhancement of Au/TiO<sub>2</sub> catalyst activity in *n*-octanol oxidation [30]. Changes in the catalytic behavior were associated with a change in the electronic state of gold caused by the surface modification of TiO<sub>2</sub> with oxides of magnesium and iron. However, the obtained experimental data turned out to be insufficient to identify the nature of the active site of these catalytic systems.

Therefore, in this work we aimed to study, in detail, how various electronic states of gold are formed under several factors, such as gold loading, treatment atmosphere, modifier nature, and how they affect the catalytic performance of Au/M<sub>x</sub>O<sub>y</sub>/TiO<sub>2</sub> (M<sub>x</sub>O<sub>y</sub> = Fe<sub>2</sub>O<sub>3</sub> or MgO) catalysts in *n*-octanol oxidation under mild conditions.

## 2. Materials and Methods

Commercial nonporous TiO<sub>2</sub> P25 (Evonik Degussa GmbH, Essen, Germany) was used as the initial support. Fe(NO<sub>3</sub>)<sub>3</sub>·9H<sub>2</sub>O or Mg(NO<sub>3</sub>)<sub>2</sub>·6H<sub>2</sub>O (Merck, Darmstadt, Germany) aqueous solutions

were used for the modification of titania by impregnation method. Nominal molar ratio Ti/M (M = Fe or Mg) was 40. Impregnated supports were dried at room temperature for 48 h and at 110 °C for 4 h, with following calcination at 550 °C over 4 h. According to EDS results molar ratio Ti/M was closed to nominal ones (37–39) for both modified supports, and the ratio did not change significantly after gold deposition.

The method of deposition-precipitation with urea was used for gold deposition with 0.5 and 4 wt.% nominal loadings on the supports using  $\text{HAuCl}_4 \cdot 3\text{H}_2\text{O}$  (Merck, Darmstadt, Germany) as a precursor. The process of gold deposition was conducted in the absence of light, according to the previously reported procedure [34,35]. Shortly, the support was added in an aqueous solution (distilled water) containing  $4.2 \times 10^{-3}$  M of the gold precursor and 0.42 M urea (Merck, Darmstadt, Germany). This mixture had an initial pH of 2.4. After heating of solution at 80 °C for 16 h, the pH was adjusted to 7.5. The solution was then centrifuged at 11,000 rpm for 15 min and decanted, and the remaining solid washed with water; this procedure was repeated 4 times. The final stage was drying of samples under vacuum 2 h at 80 °C. Such samples before any pretreatment ( $\text{H}_2$  or  $\text{O}_2$  atmosphere) will be denoted herein as as-prepared samples. To prevent any alteration, the samples were stored in a desiccator under vacuum, away from light and at room temperature.

Nitrogen adsorption-desorption isotherms at  $-196$  °C were used for the study of textural properties of catalysts and supports. Micromeritics TriStar 3000 apparatus (Norcross, GA, USA) was applied for the record of isotherms. Degassing of samples under vacuum at 300 °C for 5 h preceded each measurement. Normalization to standard temperature and pressure of adsorbed  $\text{N}_2$  volume was carried out. The BET method was applied to the nitrogen adsorption data ( $P/P_0$  range 0.05–0.25) for the calculation of the specific surface area ( $S_{\text{BET}}$ ) of the samples.

XRD patterns were obtained by using a Philips XPert PR diffractometer (Amsterdam, The Netherlands) using Ni-filtered  $\text{CuK}\alpha$  ( $\lambda = 0.15406$  nm) radiation. The step-scanning procedure included the following parameters (step size  $0.02^\circ$ ; 0.5 s).

Scanning transmission electron microscopy-high angle annular dark field (STEM-HAADF) measurements were conducted with a microscope (JEOL JEM-2100F, JEOL Ltd., Tokyo, Japan) operated at 200 kV. Prior to study, samples were abraded to a fine powder state and then, a drop of the suspension was deposited on a lacey carbon coated copper grid. For each sample, at least ten representative images from the microscope were acquired, and at least 150 particles for each sample were taken into account for obtaining particle size distribution. Gold contents were measured by energy dispersive spectroscopy (XEDS) in the same system of the microscope equipped with an Oxford INCA X-sight system detector (Oxford Instruments, Abingdon, Oxfordshire, UK).

XPS was applied for the study of gold electronic state on catalyst surface with a SPECS GmbH (SPECS Surface Nano Analysis GmbH, Berlin, Germany) custom-made system using a PHOIBOS 150 WAL hemispherical analyzer and a non-monochromated X-ray source (Al  $\text{K}\alpha$  X-rays 1486.6 eV, 200 W). Detailed information was given in our previous papers [31,32].

Diffuse reflectance Fourier transform infrared spectroscopy (DRIFTS) measurements were performed on a Bruker EQUINOX 55/S FTIR spectrometer (Bruker Optik GmbH, Ettlingen, Germany) equipped with a homemade accessory. All DRIFTS CO spectra on the catalyst samples were recorded at 20 Torr pressure (5% accuracy measurement), at room temperature with a resolution of  $4 \text{ cm}^{-1}$ . Typically, the powdered sample was loaded in a quartz ampoule with a window of  $\text{CaF}_2$ . Prior to measurements, the samples were calcined at 100 °C under vacuum ( $10^{-4}$  Torr) for 1 h. Then, each catalyst was studied in three states: as-prepared, and after pretreatments either in  $\text{H}_2$  or in  $\text{O}_2$  at 300 °C for 1 h at 100 Torr, and then cooled down to room temperature. After that, hydrogen or oxygen was evacuated and CO adsorption (>99%) was carried out. The obtained DRIFTS data were presented in the form of Kubelka–Munk units (KMU). DRIFT CO spectra were obtained by subtracting the CO gas phase spectrum and the baseline was corrected. Pure supports did not exhibit bands of adsorbed CO in this region of the spectrum under the mentioned conditions.

NH<sub>3</sub>-temperature-programmable desorption (TPD) and CO<sub>2</sub>-TPD methods were applied to the study of acid and basic properties of the catalysts and corresponding supports on a “Chemosorb” chemisorption analyzer (Neosib, Novosibirsk, Russia), equipped with a thermal conductivity detector (TCD), which was calibrated with NH<sub>3</sub> or CO<sub>2</sub> prior to analysis. The starting desorption temperature in the case of CO<sub>2</sub> was 25 °C, while TPD of ammonia started from 100 °C. Additionally, carrier gas in NH<sub>3</sub>-TPD was helium; in CO<sub>2</sub>-TPD was argon. Otherwise, the experimental procedure was the same in both cases, except for the listed differences in these methods. Prior to the measurements, the samples were treated at 300 °C under an inert atmosphere (He or Ar) for 1 h, to remove the impurities adsorbed on the surface. Then, the temperature was decreased to 100 °C or 25 °C, followed by saturation with NH<sub>3</sub> or CO<sub>2</sub> for 1 h and flushing with He or Ar for 1 h, to remove physisorbed ammonia or carbon dioxide. After that, the temperature was increased to 600 °C at a rate of 10 °C min<sup>-1</sup>, under an inert atmosphere. For a comparative analysis, NH<sub>3</sub> and CO<sub>2</sub> desorption profiles of catalysts are divided into three temperature ranges: 100 (25)–200 °C, 200–400 °C and 400–600 °C, and are assigned to weak, medium and strong acid or basic sites, respectively.

Before catalytic experiments of oxidation of *n*-octanol (Merck, ≥99%, HPLC grade), as-prepared samples were treated either in O<sub>2</sub> atmosphere (herein denoted as *n*% Au/(M<sub>x</sub>O<sub>y</sub>)/TiO<sub>2</sub>\_pO<sub>2</sub>) or in H<sub>2</sub> atmosphere (herein denoted as *n*% Au/(M<sub>x</sub>O<sub>y</sub>)/TiO<sub>2</sub>\_pH<sub>2</sub>) at 300 °C for 1 h, where *n* is the gold content in wt.% and M is the metal (Fe or Mg) of the modifier oxide.

The catalytic properties were studied at the temperature 80 °C under atmospheric conditions for 6 h in a semi-batch reactor, which is a four-necked round bottom flask equipped with reflux, oxygen feed, thermocouple and a septum cap. The appropriate amount of catalyst sample in *n*-octanol/Au ratio = 100 mol/mol was added to a flask with 0.1 M solution of *n*-octanol (25 mL) in *n*-heptane (Supelco, ≥99%, HPLC grade). Oxygen was bubbled through the reaction mixture with 30 mL/min rate. To monitor the reaction progress, small aliquots of the reacting mixture by using nylon syringe filters (pore 0.45 μm) were collected at 0.25, 0.5, 1, 2, 4 and 6 h, and then were analyzed in a Varian 450 gas chromatograph (Varian Inc, Palo Alto, CA, USA) with flame ionization detector (FID), using a capillary DB wax column (15 m × 0.548 mm, Varian Inc., Palo Alto, CA, USA), and He as the carrier gas. The attribution of peaks was made by comparison with chromatograms of genuine samples. In the absence of support/catalyst, no activity was observed in oxidation of *n*-octanol.

Alcohol conversion (*X*) and product yield (*Y<sub>i</sub>*) and selectivity (*S<sub>i</sub>*) were calculated in terms of moles of C atoms, as follows:

$$Y_i = \frac{n_i C_i}{8 \cdot C_{ROH}^{in}} \cdot 100 \quad (1)$$

where *n<sub>i</sub>* is the number of carbon atoms in compound *i*, and *C<sub>i</sub>* is its molar concentration, and *C<sub>ROH<sup>in</sup></sub>* represents initial octanol concentration.

Conversion was calculated as the sum of the yields of carbon containing products, and product selectivity as the ratio between product yield and conversion.

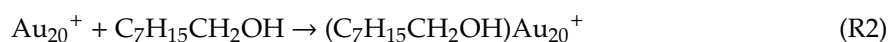
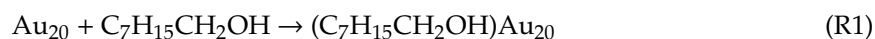
$$X_{ROH} = \sum Y_i \quad (2)$$

$$S_i = \frac{Y_i}{X_{ROH}} \cdot 100 \quad (3)$$

Carbon balances in all reported data were within 100 ± 3%.

The adsorption of *n*-octanol on gold nanoparticles was simulated using the density functional theory PBE [36] to determine at the atomic level the type of adsorption sites (Au<sup>0</sup> or Au<sup>+</sup>, top atom or facet atom) of nanogold catalysts. As a model of nanoparticles, the tetrahedral Au<sub>20</sub> cluster was considered. The experimentally observed Au<sub>20</sub> cluster is 1 nm in size [37]. Because the cluster has atoms with different coordination numbers (on the top, on the facet and on the edge), it has been a popular model for studying the structural effects in adsorption and catalysis [38,39].

We simulated the *n*-octanol adsorption as a reaction:

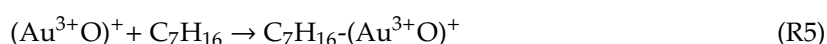
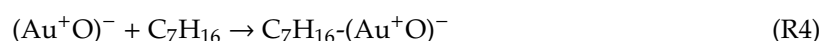
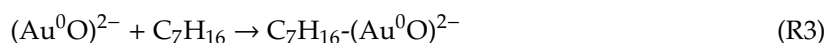


The different coordination of alcohol on  $\text{Au}_{20}$  was considered. The structures of  $(\text{C}_7\text{H}_{15}\text{CH}_2\text{OH})\text{Au}_{20}$  were optimized, and the total energies of the reagents and products were calculated, taking into account the energy of zero vibrations. The change in total energy and standard enthalpies of the Reactions (R1) and (R2) at the 100 °C temperature were determined according to the formulas:

$$\Delta E_1 = E(\text{octanol-Au}_{20}) - E(\text{Au}_{20}) - E(\text{octanol}) \quad (4)$$

$$\Delta E_2 = E(\text{octanol-Au}_{20}^+) - E(\text{Au}_{20}^+) - E(\text{octanol}) \quad (5)$$

To reveal the role of different gold sites in the adsorption of solvent molecules, heptane adsorption on simple  $(\text{Au}^0\text{O})^{2-}$ ,  $(\text{Au}^+\text{O})^-$ , and  $(\text{Au}^{3+}\text{O})^+$  models containing  $\text{Au}^0$ ,  $\text{Au}^+$ , and  $\text{Au}^{3+}$  was also studied at the atomic level using density functional theory calculation with PBE functional [36]. We simulated  $\text{C}_7\text{H}_{16}$  adsorption through Reactions (R3)–(R5):



The structures of all molecules were fully optimized, and the total energies of the reagents and products were calculated taking into account the energy of zero vibrations. Adsorption energies were calculated as the difference in total energies of adsorbed complex and the reagents (heptane and  $(\text{Au}^0\text{O})^{2-}/(\text{Au}^+\text{O})^-/(\text{Au}^{3+}\text{O})^+$ ).

All density functional theory (DFT) calculations were performed in the PRIRODA program (version 17, Russia) [40], using a Lomonosov supercomputer [41].

### 3. Results and Discussion

#### 3.1. Catalytic Results

The results showed that the gold content, support nature and the pretreatment atmosphere significantly affected the catalytic properties of gold catalysts in the liquid phase oxidation of *n*-octanol. The activity of catalysts in the as-prepared state was insignificant and practically does not depend on the nature of the support and gold content. The reason for this is that gold in as-prepared samples is found on the support surface in the form of a trivalent gold complex with urea hydrolysis products, which is catalytically inactive [30,42].

However, for most of the studied catalysts, the activity increased several times after either the reduction or oxidation treatment. However, depending on the pretreatment atmosphere, the effect of gold content on activity was different (Figure 1). After  $\text{H}_2$  treatment, the order of activity was:  $\text{Au/MgO/TiO}_2 > \text{Au/Fe}_2\text{O}_3/\text{TiO}_2 > \text{Au/TiO}_2$ , and activity increased with an increase of gold content in the three cases (Figure 1).

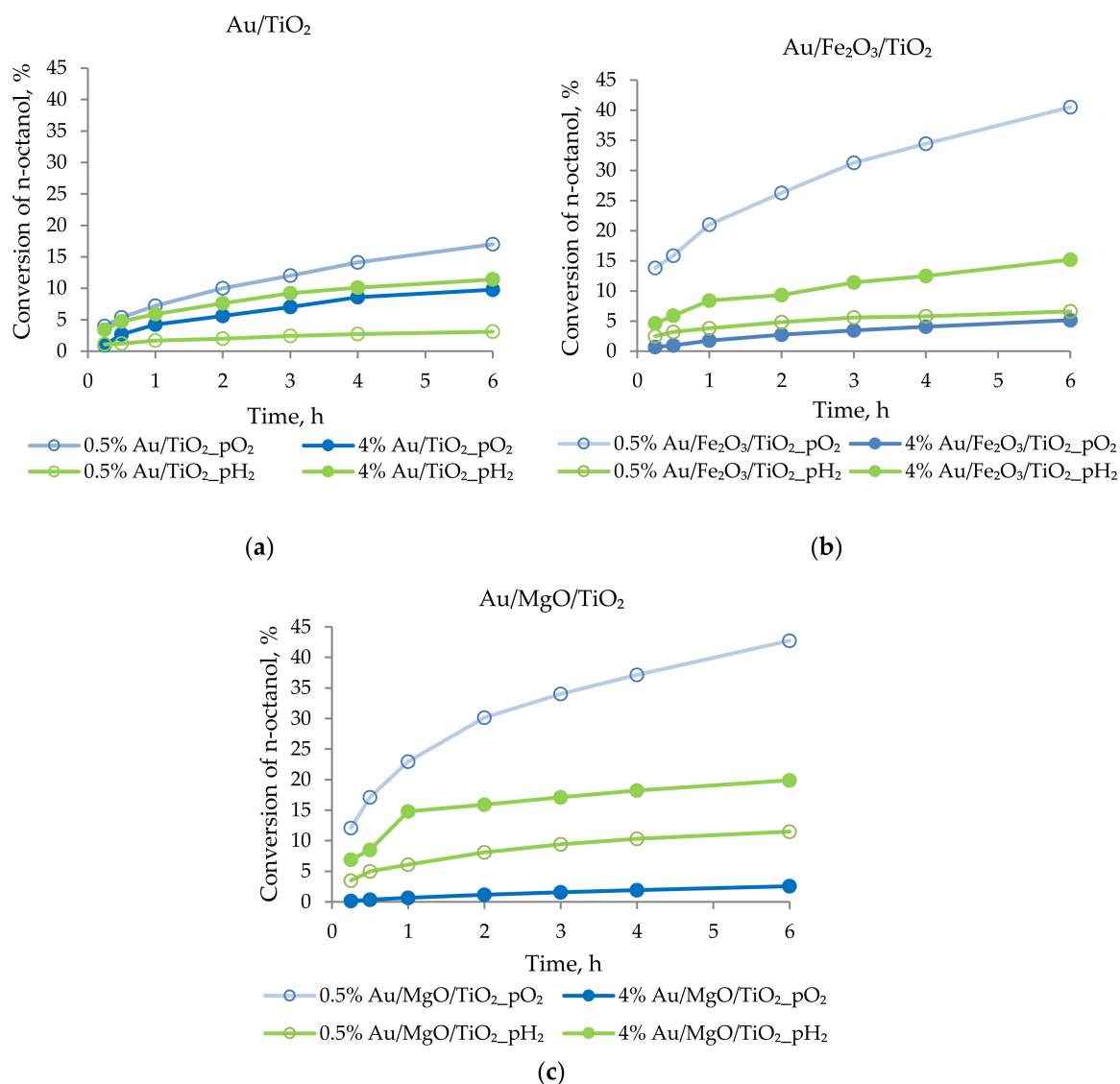


**Figure 1.** Effect of gold loading and pretreatments on the oxidation of *n*-octanol on Au/M<sub>x</sub>O<sub>y</sub>/TiO<sub>2</sub> (M<sub>x</sub>O<sub>y</sub> = Fe<sub>2</sub>O<sub>3</sub>, MgO) catalysts: evolution of conversion with run time (a–c).

Analysis of the products distribution (Figure 2) for 0.5% Au/TiO<sub>2</sub>\_pH<sub>2</sub>, 0.5% Au/Fe<sub>2</sub>O<sub>3</sub>/TiO<sub>2</sub>\_pH<sub>2</sub>, 0.5% Au/MgO/TiO<sub>2</sub>\_pH<sub>2</sub> samples showed that selectivity to acid formation (39%, 30% and 53% respectively) increased with run time, while selectivity to aldehyde sharply decreased from 100% at the reaction start down to 50% for 0.5% Au/TiO<sub>2</sub>\_pH<sub>2</sub>, 53% for 0.5% Au/Fe<sub>2</sub>O<sub>3</sub>/TiO<sub>2</sub>\_pH<sub>2</sub> and 30% for 0.5% Au/MgO/TiO<sub>2</sub>\_pH<sub>2</sub>. Ester formation was at 12% and 17% levels for unmodified sample and modified samples, respectively. The selectivity trends were totally different for their homologues with 4 wt.% gold loading after hydrogen pretreatment. The main product was octanal. Octanoic acid formation was practically negligible; only some traces of acid were detected at longer run times for 4% Au/TiO<sub>2</sub>\_pH<sub>2</sub> and 4% Au/MgO/TiO<sub>2</sub>\_pH<sub>2</sub>. For 4% Au/Fe<sub>2</sub>O<sub>3</sub>/TiO<sub>2</sub>\_pH<sub>2</sub>; selectivity towards octyl octanoate increased at the expense of octanal formation with no acid formation.

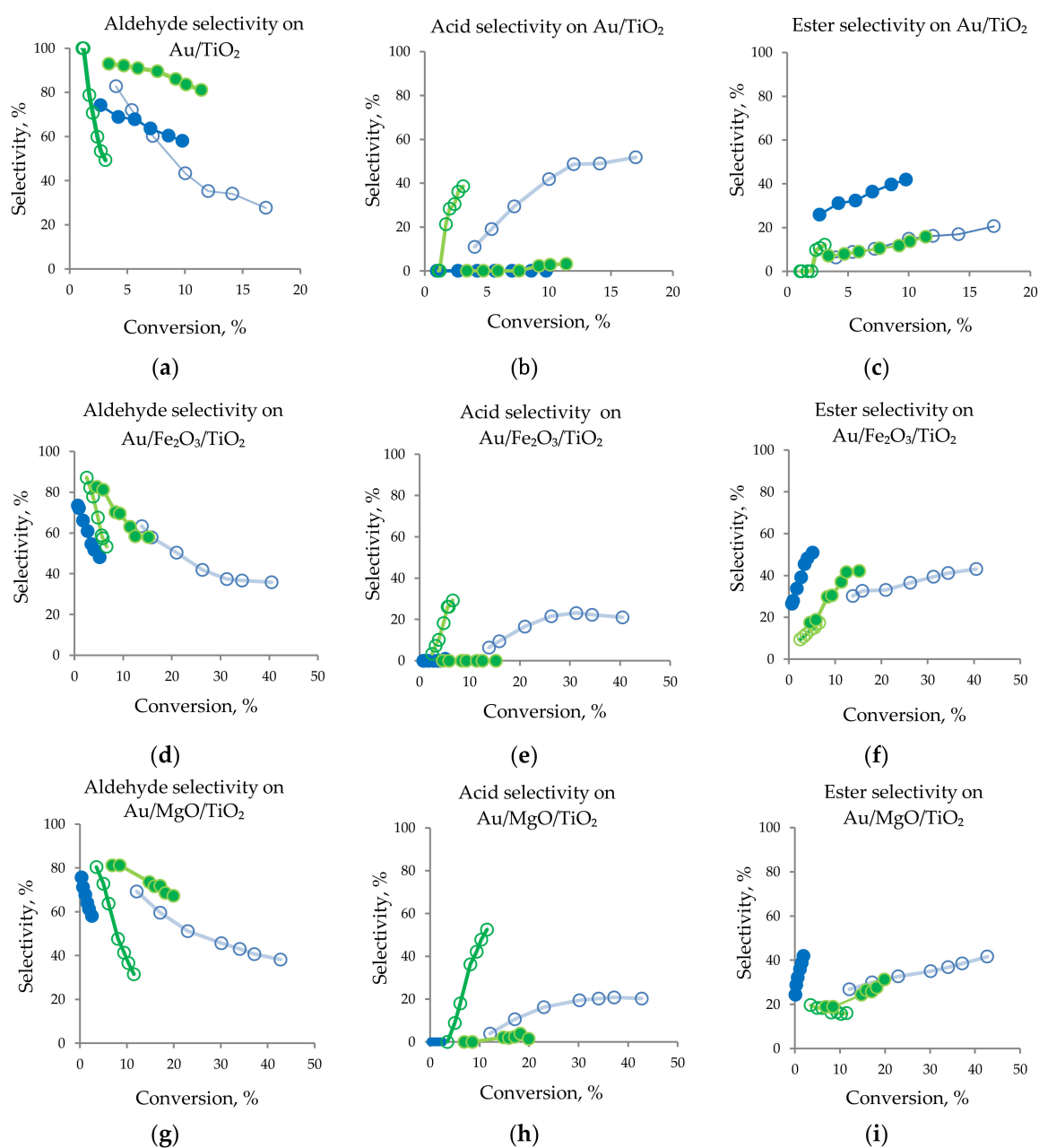
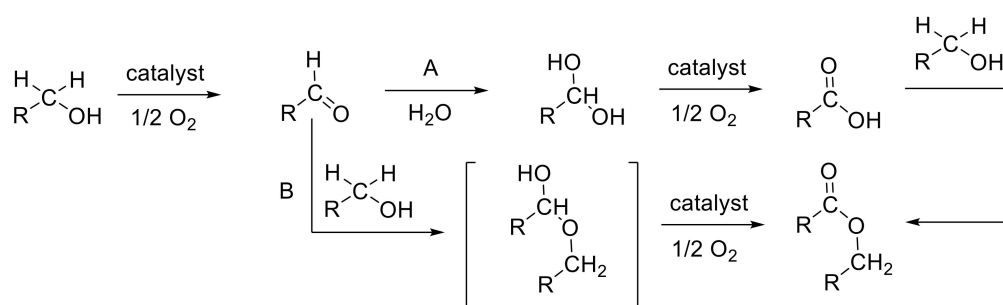


**Figure 2.** Effect of gold loading and pretreatments on the oxidation of *n*-octanol on Au/ $M_xO_y$ /TiO<sub>2</sub> ( $M_xO_y = Fe_2O_3, MgO$ ) catalysts. Products selectivity evolution with conversion for Au/TiO<sub>2</sub> (a–c), Au/Fe<sub>2</sub>O<sub>3</sub>/TiO<sub>2</sub> (d–f) and Au/MgO/TiO<sub>2</sub> (g–i) is shown. Green lines: results after hydrogen pretreatment, blue lines: after oxygen pretreatment. Catalysts Au contents: hollow symbols show catalysts with 0.5% Au; full symbols with 4% Au.

Such changes in the reaction product distribution with an increase in Au content should be caused by alteration in the acid-base properties of support. Aldehyde formation requires only the first step of the reaction mechanism, that occurs on the gold active surface, while the formation of octanoic acid and octyl octanoate requires a second mechanistic step [29,30] through intermediates formed by acid-base catalyzed reactions, proceeding mainly on the support surface. In addition, in the scheme proposed by several authors [29–33,43], the formation of ester or acid can occur by two routes: hydration to a geminal diol (Scheme 1, A) that can be further oxidized to octanoic acid, or an acetalization to form the hemiacetal, that can be oxidized to octyl octanoate. The ester could also be formed by the esterification of the acid with the alcohol (Scheme 1, B).





**Scheme 1.** Possible reaction pathways for the oxidation of *n*-octanol on supported gold catalysts (adapted from [29–33,43]).

In contrast, after pretreatment of samples in an oxygen atmosphere, the opposite dependence on the activity of the gold content was observed, i.e., the catalytic activity decreased with the increase of gold content for all supports. Similarly good results were achieved using modified samples with the lower Au content after oxidation pretreatment at 300 °C for 1 h, namely 0.5% Au/MgO/TiO<sub>2</sub>-pO<sub>2</sub> and 0.5% Au/Fe<sub>2</sub>O<sub>3</sub>/TiO<sub>2</sub>-pO<sub>2</sub>: the conversion of *n*-octanol after 6 h reached 43% and 41%, respectively, with increasing ester selectivity in both cases (Figures 1 and 2). Acid formation (up to 52% selectivity) was observed only for the unmodified catalyst, 0.5% Au/TiO<sub>2</sub>-pO<sub>2</sub>. In case of modified samples, acid formation decreased after 3 h of reaction and was 20% after 6 h for both catalysts.

For catalysts with higher gold loading after oxygen treatment, similar trends in selectivity can be seen for samples with samples after hydrogen treatment: almost complete absence of acid (1% of acid was found only for 4% Au/Fe<sub>2</sub>O<sub>3</sub>/TiO<sub>2</sub>-pO<sub>2</sub>). However, the difference is a larger formation of ester: 20% in case of 4% Au/TiO<sub>2</sub>-pO<sub>2</sub>, 40% and 42%, in case of 4% Au/MgO/TiO<sub>2</sub>-pO<sub>2</sub> and 4% Au/Fe<sub>2</sub>O<sub>3</sub>/TiO<sub>2</sub>-pO<sub>2</sub>, respectively. At the same time, it is worth noting that the activity of these catalysts was very low, especially for modified samples (Figure 1b,c).

A common feature of catalysts with 0.5% Au, independently of the pretreatment, was the preferential formation of acid, but a larger tendency to ester formation was found for catalysts with oxygen pretreatment; also 0.5% Au/MgO/TiO<sub>2</sub> and 0.5% Au/Fe<sub>2</sub>O<sub>3</sub>/TiO<sub>2</sub> catalysts showed almost identical activity and selectivity in *n*-octanol oxidation.

### 3.2. Catalysts Characterization

To understand the differences observed in the catalytic behavior of the samples, a series of physicochemical studies were carried out.

The XRD method was used to study the phase composition of the catalysts. The diffractograms (Figure 3) showed the absence of diffraction lines related to gold or the modifiers, indicating either small sizes of Au particles and metal oxides (lower than the XRD sensitivity threshold of 3–4 nm) [44] or their X-ray amorphous structure.

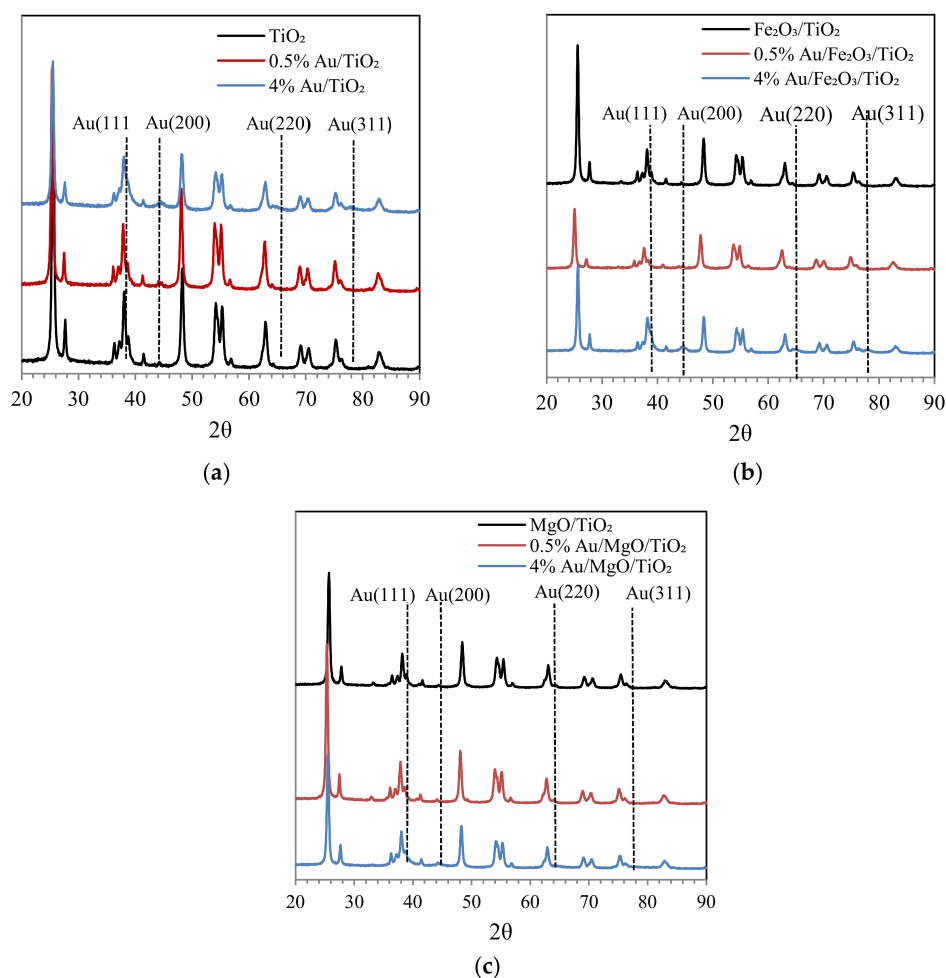
Table 2 summarizes the specific surface area (*S*<sub>BET</sub>) and gold content of the catalysts and their corresponding supports. Because of modification with both Fe and Mg oxides, *S*<sub>BET</sub> of the initial TiO<sub>2</sub> support was reduced by 13% (48–49 m<sup>2</sup>/g). Further gold deposition did not significantly change the supports' *S*<sub>BET</sub>, except for catalysts with 4% Au, where *S*<sub>BET</sub> had a 10% decrease. Elemental analysis showed that the actual gold loadings obtained were close to the nominal value.

Table 2 also depicts the Au particle size obtained from STEM HAADF images presented in Figure 4. The distribution of gold nanoparticles for all the studied catalysts is in the range of 1–10 nm, with the exception of 0.5% Au/TiO<sub>2</sub>-pH<sub>2</sub>, for which larger particles were observed; up to 15 nm (Figure 4a). The average size of Au NPs was found within the 2.6–5.2 nm interval for the studied materials (Table 2). The most active samples, namely 0.5% Au/Fe<sub>2</sub>O<sub>3</sub>/TiO<sub>2</sub>-pO<sub>2</sub> and 0.5% Au/MgO/TiO<sub>2</sub>-pO<sub>2</sub>, with almost equal conversion (41% and 43%) had similar mean particle size (3.4 and 3.2 nm), respectively. However, catalysts with smaller particle sizes, like 0.5% Au/MgO/TiO<sub>2</sub>-pH<sub>2</sub> (2.6 nm) and 4% Au/MgO/TiO<sub>2</sub>-pO<sub>2</sub>

(2.9 nm), demonstrated low activity in *n*-octanol oxidation (12% and 3% conversion, respectively). Therefore, taking into account the data from catalytic studies, no direct correlation between Au NPs average size and catalytic performance can be found.

**Table 2.** Textural properties of supports and catalysts, analytical content and particle size of Au. Data for Entries 1–4 taken from [31,32].

Entry	Sample	$S_{\text{BET}}$ , m <sup>2</sup> /g		EDX Au Content, wt. %	Au Average Particle Size, nm
		Support	Catalyst		
1	0.5% Au/TiO <sub>2</sub> _pH <sub>2</sub>	55	54	0.4	4.4
2	0.5% Au/TiO <sub>2</sub> _pO <sub>2</sub>	55	54	0.4	4.2
3	4% Au/TiO <sub>2</sub> _pH <sub>2</sub>	55	50	4.0	3.0
4	4% Au/TiO <sub>2</sub> _pO <sub>2</sub>	55	50	4.0	3.3
5	0.5% Au/MgO/TiO <sub>2</sub> _pH <sub>2</sub>	48	47	0.3	2.6
6	0.5% Au/MgO/TiO <sub>2</sub> _pO <sub>2</sub>	48	47	0.3	3.2
7	4% Au/MgO/TiO <sub>2</sub> _pH <sub>2</sub>	48	43	4.0	5.1
8	4% Au/MgO/TiO <sub>2</sub> _pO <sub>2</sub>	48	43	4.0	2.9
9	0.5% Au/Fe <sub>2</sub> O <sub>3</sub> /TiO <sub>2</sub> _pH <sub>2</sub>	49	49	0.5	3.1
10	0.5% Au/Fe <sub>2</sub> O <sub>3</sub> /TiO <sub>2</sub> _pO <sub>2</sub>	49	49	0.5	3.4
11	4% Au/Fe <sub>2</sub> O <sub>3</sub> /TiO <sub>2</sub> _pH <sub>2</sub>	49	44	3.2	5.2
12	4% Au/Fe <sub>2</sub> O <sub>3</sub> /TiO <sub>2</sub> _pO <sub>2</sub>	49	44	3.2	3.2



**Figure 3.** XRD patterns for catalysts Au/TiO<sub>2</sub> (a), Au/Fe<sub>2</sub>O<sub>3</sub>/TiO<sub>2</sub> (b), Au/MgO/TiO<sub>2</sub> (c) treated in H<sub>2</sub> (300 °C, 1 h) and their corresponding supports.

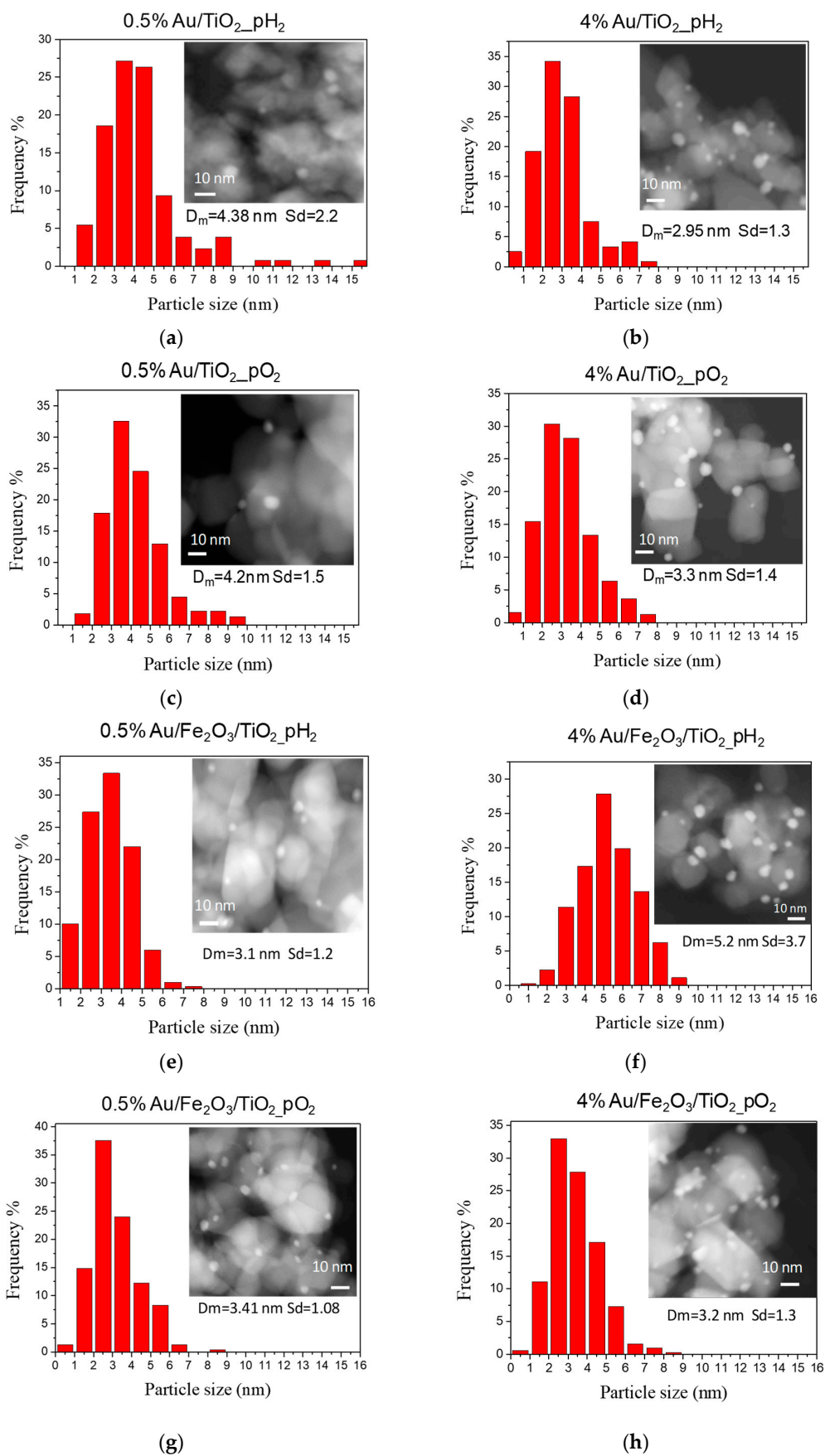
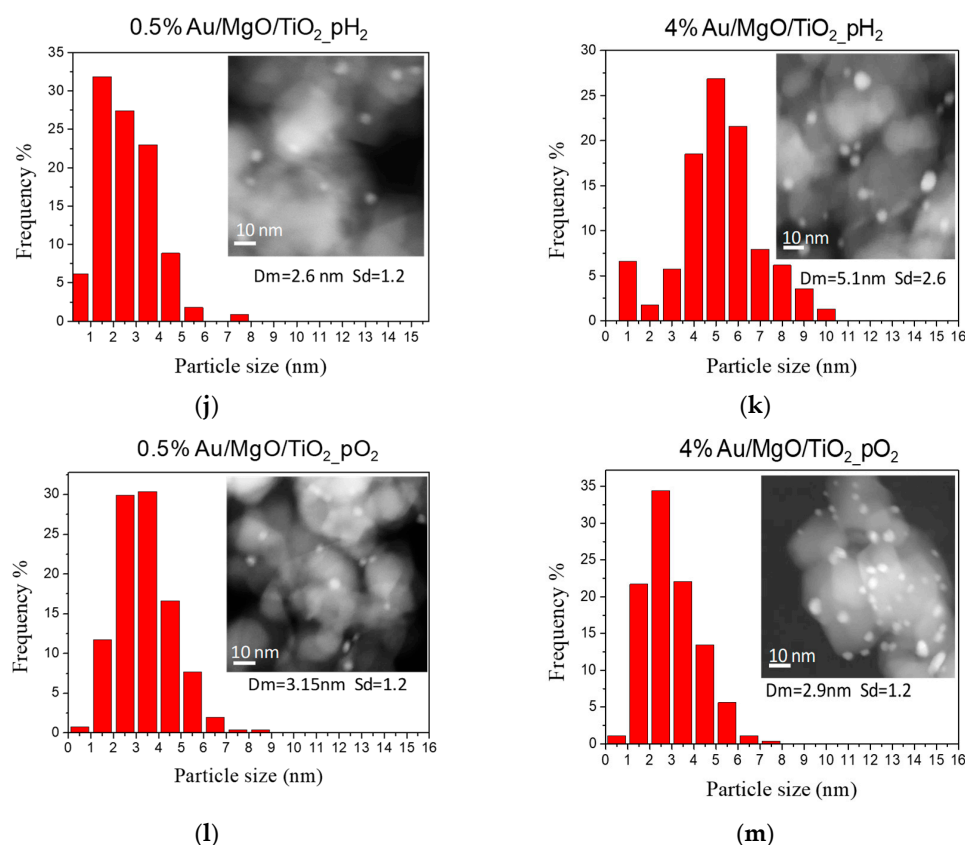


Figure 4. Cont.



**Figure 4.** Au particle size distribution and representative STEM HAADF micrographs of catalysts Au/TiO<sub>2</sub> (a–d), Au/Fe<sub>2</sub>O<sub>3</sub>/TiO<sub>2</sub> (e–h), Au/MgO/TiO<sub>2</sub> (j–m), for different gold amounts (0.5 or 4 wt.%) and pretreatment atmospheres (H<sub>2</sub> or O<sub>2</sub>).

Nevertheless, one should note that according to DRIFT CO studies and XPS presented below (Table 3, Figures 5 and 6), there is a fraction of gold in ionic state (Au<sup>+</sup> or Au<sup>3+</sup>), which is not detected by STEM. The amount of these gold species depends on the support, pretreatment and gold content. Furthermore, for such a type of reaction, not all metal particles visible on the micrographs are active participants in the catalytic process; in some cases, only particles with a size below the threshold of the technique (1 nm) and less are active, as reported in the literature and in our previous works [29,30,45–47].

**Table 3.** Effect of gold content (0.5 or 4 wt.%) and redox treatment (H<sub>2</sub> or O<sub>2</sub>) on the different electronic states of Au (determined by XPS), and their catalytic activity for *n*-octanol oxidation for Au/TiO<sub>2</sub>, Au/Fe<sub>2</sub>O<sub>3</sub>/TiO<sub>2</sub>, Au/MgO/TiO<sub>2</sub> catalysts. Entries 1–4 data are taken from [31,32].

Entry	Catalyst	Au Electronic State Relative Content, %			Conversion of <i>n</i> -Octanol after 6 h, %
		Au <sup>0</sup>	Au <sup>+</sup>	Au <sup>3+</sup>	
1	0.5% Au/TiO <sub>2</sub> _pH <sub>2</sub>	91	9	0	3
2	0.5% Au/TiO <sub>2</sub> _pO <sub>2</sub>	84	16	0	17
3	4% Au/TiO <sub>2</sub> _pH <sub>2</sub>	73	14	11	11
4	4% Au/TiO <sub>2</sub> _pO <sub>2</sub>	89	11	0	6
5	0.5% Au/MgO/TiO <sub>2</sub> _pH <sub>2</sub>	81	11	8	12
6	0.5% Au/MgO/TiO <sub>2</sub> _pO <sub>2</sub>	67	25	8	43
7	4% Au/MgO/TiO <sub>2</sub> _pH <sub>2</sub>	51	29	20	20
8	4% Au/MgO/TiO <sub>2</sub> _pO <sub>2</sub>	100	0	0	3
9	0.5% Au/Fe <sub>2</sub> O <sub>3</sub> /TiO <sub>2</sub> _pH <sub>2</sub>	28	29	43	7
10	0.5% Au/Fe <sub>2</sub> O <sub>3</sub> /TiO <sub>2</sub> _pO <sub>2</sub>	26	64	10	41
11	4% Au/Fe <sub>2</sub> O <sub>3</sub> /TiO <sub>2</sub> _pH <sub>2</sub>	42	37	21	15
12	4% Au/Fe <sub>2</sub> O <sub>3</sub> /TiO <sub>2</sub> _pO <sub>2</sub>	100	0	0	5

The XPS method was applied to investigate gold electronic states on the support surface. The binding energies of Au 4f spectra according to XPS measurements show various states of gold, ions  $\text{Au}^+$  and  $\text{Au}^{3+}$  and neutral gold, which were affected by the support composition, pretreatment atmosphere, and Au content (Table 3). The XPS spectra for modified samples are presented in Figure 5.

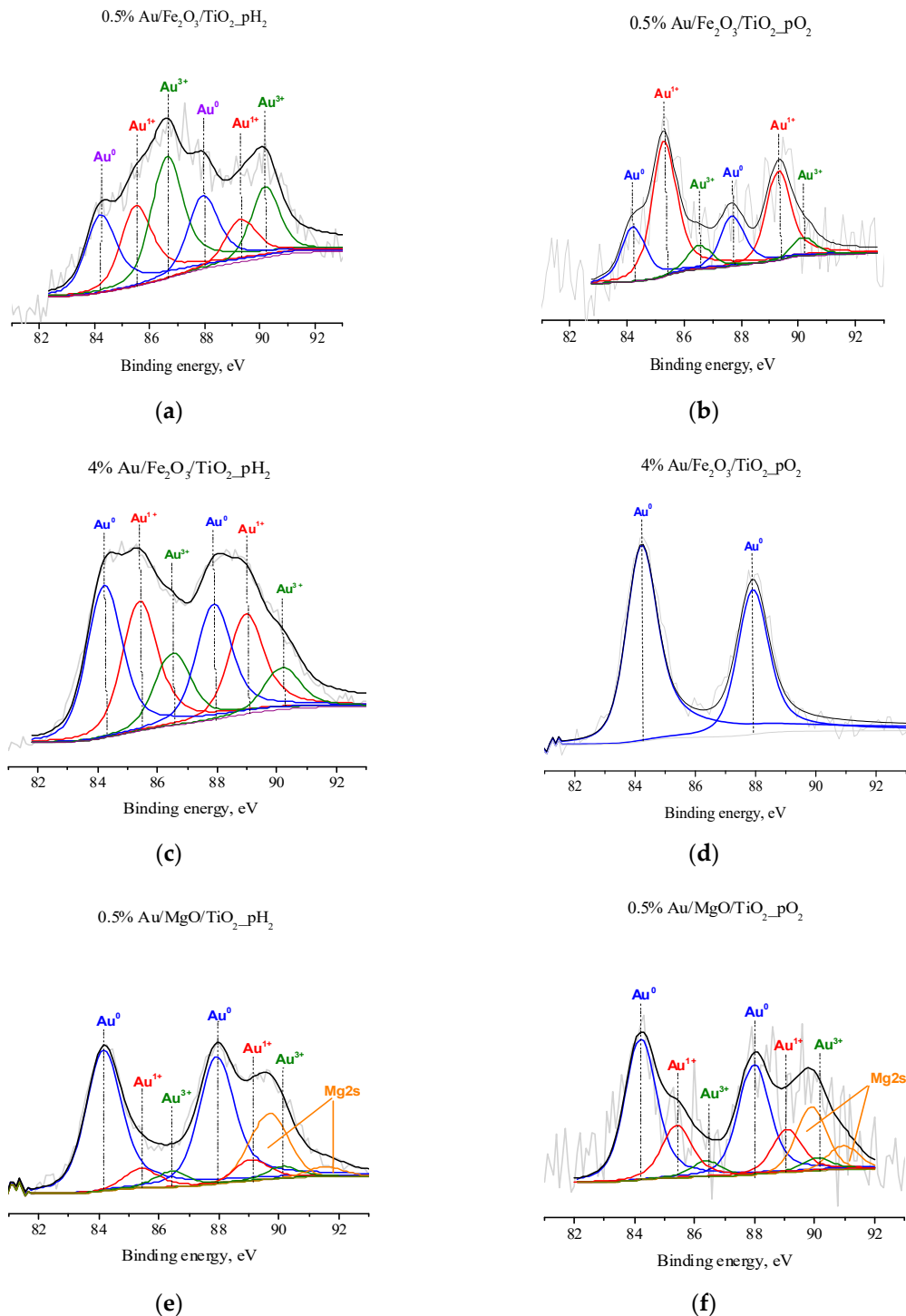
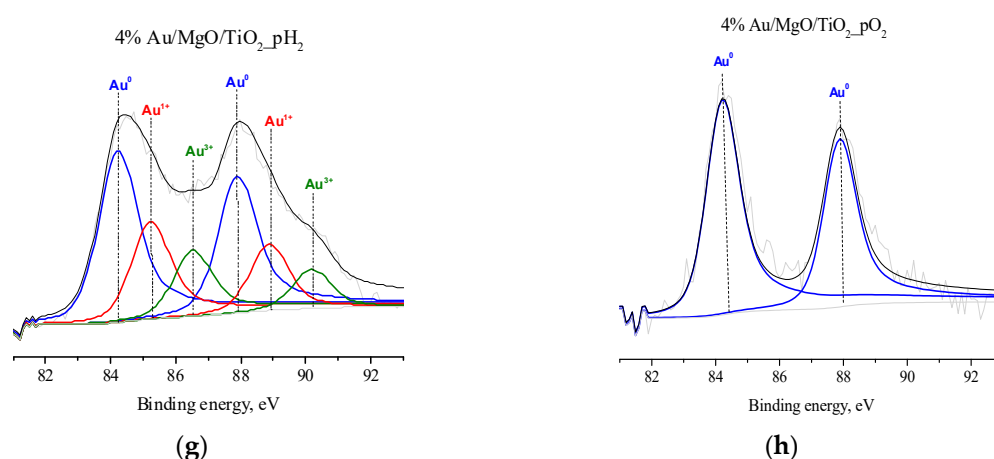


Figure 5. Cont.



**Figure 5.** Au4f XP spectra of Au/Fe<sub>2</sub>O<sub>3</sub>/TiO<sub>2</sub> and Au/MgO/TiO<sub>2</sub> samples with different gold contents (0.5 or 4 wt.%), pretreated in H<sub>2</sub> or O<sub>2</sub> flow, at 300 °C, for 1 h: 0.5% Au/Fe<sub>2</sub>O<sub>3</sub>/TiO<sub>2</sub>\_pH<sub>2</sub> (a), 0.5% Au/Fe<sub>2</sub>O<sub>3</sub>/TiO<sub>2</sub>\_pO<sub>2</sub> (b), 4% Au/Fe<sub>2</sub>O<sub>3</sub>/TiO<sub>2</sub>\_pH<sub>2</sub> (c), 4% Au/Fe<sub>2</sub>O<sub>3</sub>/TiO<sub>2</sub>\_pO<sub>2</sub> (d), 0.5% Au/MgO/TiO<sub>2</sub>\_pH<sub>2</sub> (e), 0.5% Au/MgO/TiO<sub>2</sub>\_pO<sub>2</sub> (f), 4% Au/MgO/TiO<sub>2</sub>\_pH<sub>2</sub> (g), 4% Au/MgO/TiO<sub>2</sub>\_pO<sub>2</sub> (h).

All samples showed BE (Au4f<sub>7/2</sub>) 84.2 eV (26–100% relative content), attributed to Au<sup>0</sup> states [48–52]; this metallic gold was the only state found for 4% Au/MgO/TiO<sub>2</sub>\_pO<sub>2</sub> and 4% Au/Fe<sub>2</sub>O<sub>3</sub>/TiO<sub>2</sub>\_pO<sub>2</sub>. Besides the peak due to the metallic gold, another Au4f<sub>7/2</sub> peak in the BE range 85.2–85.5 eV, attributed to single charged ions (Au<sup>+</sup>) [49–52], was detected in all the other catalysts, with 9–64% relative content. The highest amount of Au<sup>+</sup> was found in the modified samples, with 0.5% Au after oxygen treatment and 4% Au after hydrogen treatment (Table 3, Entries 6, 7, 10 and 11). The 0.5% Au/Fe<sub>2</sub>O<sub>3</sub>/TiO<sub>2</sub>\_pO<sub>2</sub> sample showed the maximum contribution of single charged ions (64%), compared with other catalysts.

Moreover, another oxidized state of gold, related to three-charged gold (Au<sup>3+</sup>) with BE in the range 86.4–86.6 eV (Au4f<sub>7/2</sub>) [53–55] was found for 4% Au/TiO<sub>2</sub>\_pH<sub>2</sub> [31], and in modified catalysts with different contents (8–43%), the highest portion of Au<sup>3+</sup> being found for 0.5% Au/Fe<sub>2</sub>O<sub>3</sub>/TiO<sub>2</sub>\_pH<sub>2</sub>.

It should be noted that in both 0.5% Au/MgO/TiO<sub>2</sub>\_pH<sub>2</sub> and 0.5% Au/MgO/TiO<sub>2</sub>\_pO<sub>2</sub> catalysts, there was an overlapping of Au4f<sub>7/2</sub> line with the Mg2s line (Figure 5e,f), leading to a complication of these peaks' interpretation, with a subsequent uncertainty. However, since the Au4f<sub>7/2</sub> line is clearly visible, the states are identified correctly.

In order to obtain more information on the gold electronic states of the catalysts, DRIFT spectroscopy of CO adsorption was used. As can be seen from Figure 6, an absorption band with the maximum in the range of 2090–2130 cm<sup>-1</sup>, corresponding to the surface carbonyl groups on gold atoms Au<sup>0</sup>-CO [56], was observed for all catalysts. The different intensities of the absorption bands corresponding to Au<sup>0</sup>-CO can be explained by carbon monoxide being very weakly adsorbed on metallic gold, due to some features of the σ-π bond in M<sup>0</sup>-CO for Au compared to other noble metals [57]. Therefore, only the highly dispersed clusters or gold atoms can be sites for the adsorption of CO.

Comparing the data on the band intensity related to Au<sup>0</sup>-CO with the STEM results, it can be seen that the average particle size for samples with low frequency absorption bands is larger than for samples with high band intensity, and the differences in signal position are due to the adsorption of CO on metal clusters of different sizes. In fact, considering the DRIFT CO results for samples with the same support and Au content but different pretreatment, e.g., 4% Au/MgO/TiO<sub>2</sub>\_pO<sub>2</sub> (Figure 6l) and 4% Au/MgO/TiO<sub>2</sub>\_pH<sub>2</sub> (Figure 6m), a higher intensity of the Au<sup>0</sup>-CO band is observed for the latter, meaning that this catalyst should have smaller particles than the former. This is confirmed by the STEM results shown in Table 2: Entry 7 (4% Au/MgO/TiO<sub>2</sub>\_pO<sub>2</sub>) 5.1 nm and Entry 8 (4% Au/MgO/TiO<sub>2</sub>\_pH<sub>2</sub>) 2.9 nm. The same correlation between the average particle size and the intensity of the absorption band of metal particles was observed for the rest of the catalysts.

Another absorption band with the maximum in the range 2150–2170  $\text{cm}^{-1}$ , related to the complexes of ions  $\text{Au}^+ \text{-CO}$  [58,59], was observed in all cases, except for 4%  $\text{Au/Fe}_2\text{O}_3/\text{TiO}_2\text{-pO}_2$  and 4%  $\text{Au/MgO/TiO}_2\text{-pO}_2$  (Figure 6c,g,l). These results are in a good agreement with XPS data, as no  $\text{Au}^+$  was detected in these catalysts (Figure 5d,h). This absorption band is less intense than the one attributed to  $\text{Au}^0 \text{-CO}$ , except for 0.5%  $\text{Au/Fe}_2\text{O}_3/\text{TiO}_2\text{-pO}_2$  (Figure 6e), which correlates well with the predominant content of  $\text{Au}^+$  (64%) found by XPS in this catalyst (Table 3, Entry 10).

Along with absorption bands at 2090–2130  $\text{cm}^{-1}$  and 2150–2170  $\text{cm}^{-1}$ , ascribed to carbonyls of metallic and singly charged gold, respectively, a third band appears within 2170–2190  $\text{cm}^{-1}$  range for 4%  $\text{Au/TiO}_2\text{-pH}_2$ , 4%  $\text{Au/Fe}_2\text{O}_3/\text{TiO}_2\text{-pH}_2$ , 4%  $\text{Au/MgO/TiO}_2\text{-pH}_2$ , 0.5%  $\text{Au/Fe}_2\text{O}_3/\text{TiO}_2\text{-pH}_2$  and 0.5%  $\text{Au/Fe}_2\text{O}_3/\text{TiO}_2\text{-pO}_2$  catalysts, its interpretation being ambiguous. In most studies, this absorption band is assigned to the adsorption of CO on monovalent gold ions, as it is believed that a higher-charged gold cation ( $\text{Au}^{3+}$ ) is very unstable, or even does not form carbonyl species. That could be caused by the following reasons: (1)  $\text{Au}^{3+}$  ions are very easily reduced with CO [60–62]; (2) since  $\text{Au}^{3+}$  ions are strongly charged, probably, trivalent ions on a support surface are usually saturated by coordination, and the evacuation at elevated temperatures will easily lead to the reduction of  $\text{Au}^{3+}$  [63].

At the same time, according to XPS (Table 3 and Figure 5),  $\text{Au}^{3+}$  was found for 4%  $\text{Au/TiO}_2\text{-pH}_2$ , 4%  $\text{Au/Fe}_2\text{O}_3/\text{TiO}_2\text{-pH}_2$ , 4%  $\text{Au/MgO/TiO}_2\text{-pH}_2$  samples, even after the reduction treatment at 300 °C. Moreover,  $\text{Au}^{3+}$  relative content in these samples is much higher than in the oxidized ones. Luengnaruemitchai et al. [55] have observed that  $\text{Au}^{3+}$  remains in  $\text{Au/Fe}_2\text{O}_3/\text{TiO}_2$  catalytic systems, even after calcination at 400 °C. Such trivalent cations could be stabilized by oxygen vacancies, formed under the action of high temperature reduction treatment during the preparation of the catalyst [64–67]. It is also worth noting that the reducibility of supports such as titania increases after the gold deposition, due to metal-support interaction. A similar mechanism for the stabilization of gold ions was proposed elsewhere [68]. In addition, it was also suggested that modification of the titania surface leads to an increase in the number of oxygen defects, which in turn increases the number of stabilized gold ions. A similar trend was observed in our study.

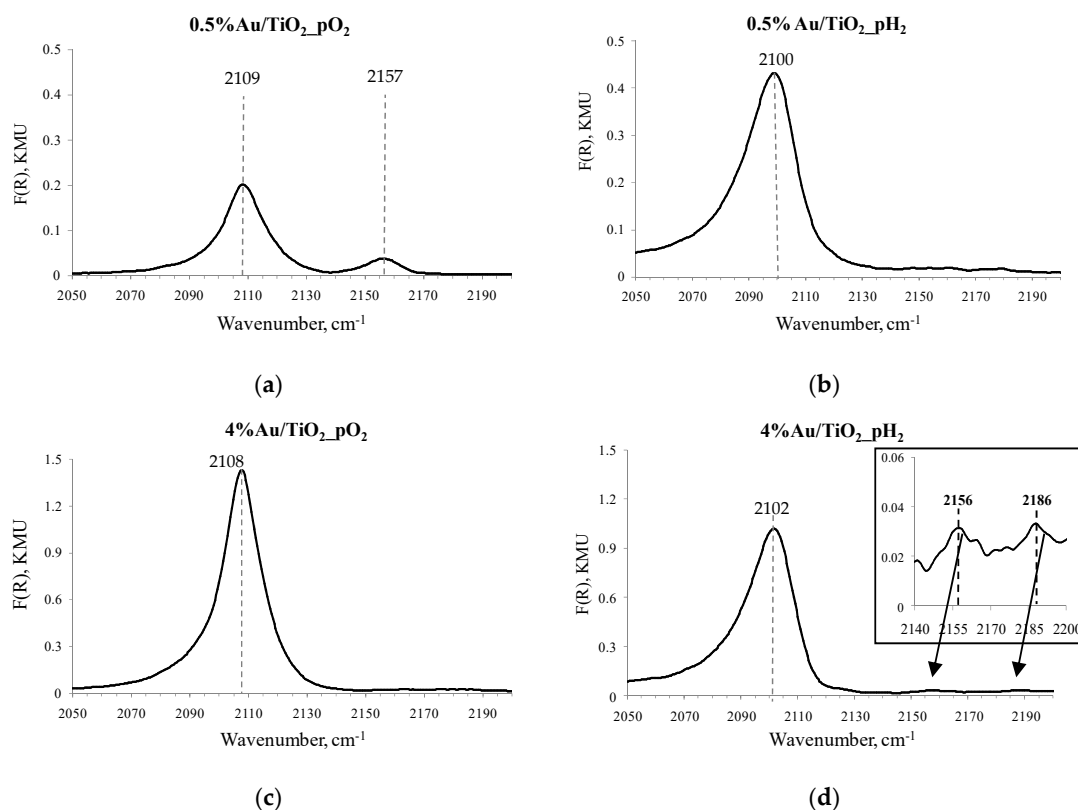
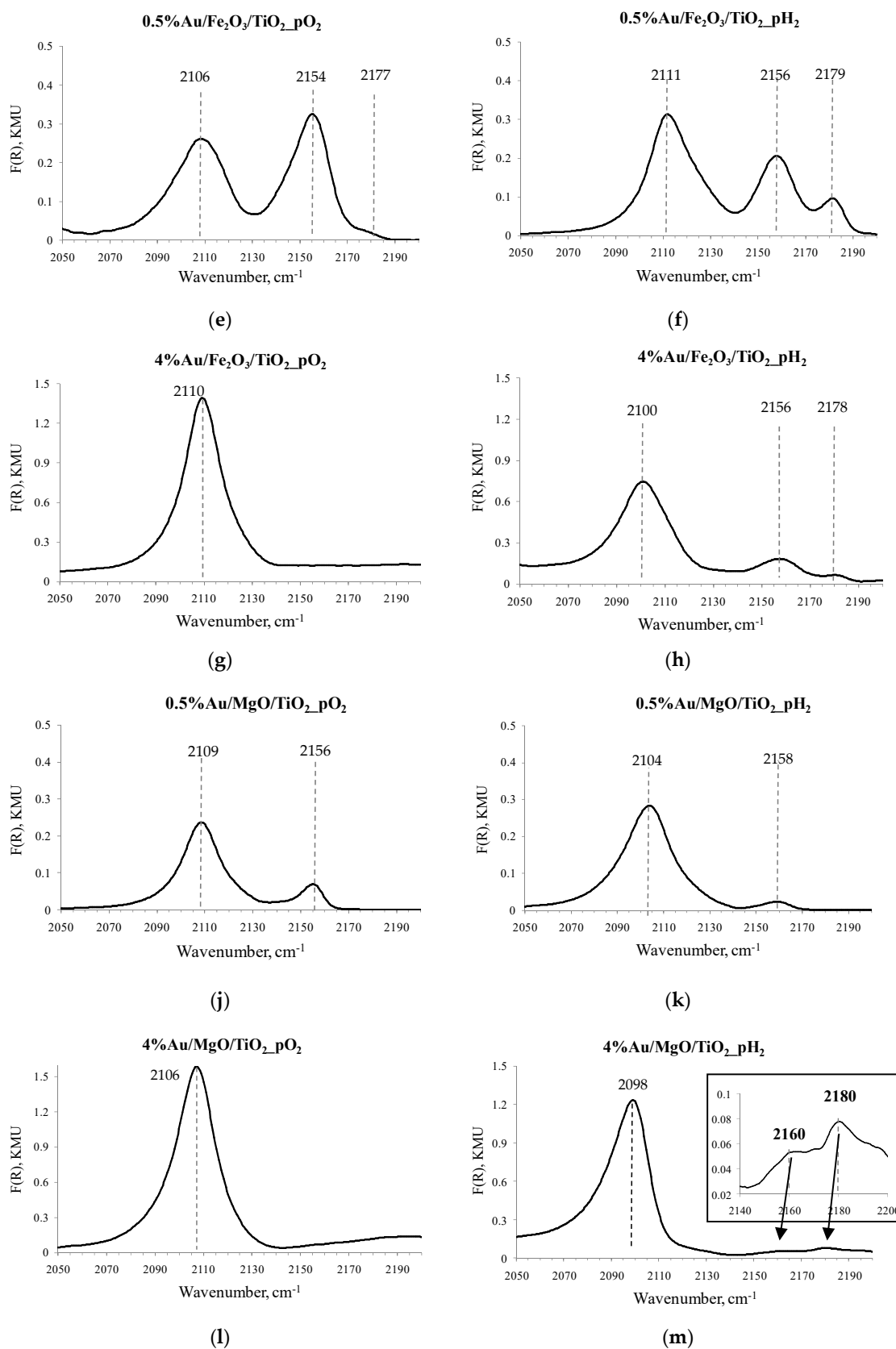


Figure 6. Cont.



**Figure 6.** DRIFT spectra of CO adsorbed on catalysts pretreated at 300 °C for 1 h under a H<sub>2</sub> or O<sub>2</sub> atmosphere.



Mihaylov et al. [63] carried out CO adsorption IR experiments for the characterization of supported gold catalysts in conditions comparable to our study, and proved that the absorption band with a maximum in the range of 2170–2190  $\text{cm}^{-1}$  corresponds to trivalent gold in non-exchange positions. Thus, we can also assume that the absorption band within 2176–2186  $\text{cm}^{-1}$  interval belongs to the trivalent gold ion. Additionally, this is in good agreement with the XPS data.

Because no direct correlation was found between the average particle size of gold and the catalytic activity of samples, and neither significant differences in the texture and structural properties of the studied catalysts were found, it can be assumed that these parameters are not determining for the observed catalytic behavior of our systems. However, another parameter capable of influencing the catalytic behavior of gold catalysts is its electronic state. Based on the analysis performed on the surface of the studied catalysts by the above methods (XPS, DRIFT CO), three electronic states of gold were found, with different relative concentrations and ratios.

Table 3 shows the relative content of the electronic states of gold found in the samples and *n*-octanol conversion after 6 h. It can be seen that there is no relationship between the conversion and the content of gold in cationic states ( $\text{Au}^+$  and  $\text{Au}^{3+}$ ), if each state is considered separately. However, if the combined concentration of  $\text{Au}^+$  and  $\text{Au}^{3+}$  is considered, one tendency can be seen: for samples with a higher concentration of  $\text{Au}^+$ , but with a lower contribution of  $\text{Au}^{3+}$ , the conversion of octanol is higher. For example, for 0.5%  $\text{Au}/\text{MgO}/\text{TiO}_2\text{-pH}_2$  and 0.5%  $\text{Au}/\text{MgO}/\text{TiO}_2\text{-pO}_2$  (Table 3, Entries 5 and 6, respectively), the  $\text{Au}^{3+}$  content is the same (8%). However, the sample after oxygen pretreatment has a larger contribution of monovalent gold (25%) than the reduced sample (11%); similarly, the conversion for  $\text{Au}/\text{MgO}/\text{TiO}_2\text{-pO}_2$  (43%) sample is much higher than for 0.5%  $\text{Au}/\text{MgO}/\text{TiO}_2\text{-pH}_2$  (12%). Furthermore, for the same content of monovalent ions (29%), in 4%  $\text{Au}/\text{MgO}/\text{TiO}_2\text{-pH}_2$  and 0.5%  $\text{Au}/\text{Fe}_2\text{O}_3/\text{TiO}_2\text{-pH}_2$  catalysts (Table 3, Entries 7 and 9, respectively), the octanol conversion is higher in the latter sample, where the content of trivalent gold is 23% lower than in the former. It is worth noting that for samples with a high content of metallic gold (Table 3, Entries 8 and 12), the conversion of *n*-octanol is very low, 3 and 5%, respectively.

Therefore, by comparing the spectroscopic and catalytic results, it can be assumed that monovalent gold ions ( $\text{Au}^+$ ) are probably responsible for enhanced catalytic activity, while metallic gold ( $\text{Au}^0$ ) and three-charged gold ( $\text{Au}^{3+}$ ) have a negative effect on the catalytic activity. The DFT calculations of *n*-octanol adsorption on tetrahedral gold clusters presented in Section 3.4 below proved that monovalent gold ions play an important role in the *n*-octanol oxidation.

The negative effect of metallic and trivalent gold on catalytic activity probably occurs due to the strong adsorption of the solvent (*n*-heptane) on both  $\text{Au}^0$  and  $\text{Au}^{3+}$  or water generated during the dehydrogenation reaction of *n*-octanol on  $\text{Au}^{3+}$  (Scheme 1). The calculations of the adsorption energy in Section 3.5 below confirmed this assumption.

### 3.3. Study of Acid-base Properties of Catalysts

$\text{CO}_2$ -TPD and  $\text{NH}_3$ -TPD methods were used to reveal which centers on the surface of the supports are responsible for the secondary reactions in the oxidation of *n*-octanol; namely, the formation of ester or acid. Three types of acid and basic sites with different concentration and strength (weak, medium and strong), depending on the temperature range where  $\text{CO}_2$  or  $\text{NH}_3$  desorption occurs, reflecting their nature, were detected for studied catalysts (Tables 4 and 5). Both basic and acid centers with weak (25–200 or 100–200  $^\circ\text{C}$ ) and medium strength (200–400  $^\circ\text{C}$ ) are usually associated with surface hydroxyl groups, i.e., the Brønsted basic centers (BBC) and Brønsted acid centers (BAC). Strong acid centers (400–600  $^\circ\text{C}$ ), along with protonated sites (hydroxyl groups), can also have aprotic nature and represent Lewis acid centers (LAC), which could include cations of gold, titanium or modifiers. Strong basic centers (400–600  $^\circ\text{C}$ ) are associated with low-coordinated oxygen anions.

Table 4. Acid properties of catalysts.

Entry	Catalyst	Concentration of Acid Centers, $\mu\text{mol/g}$			
		Weak	Medium	Strong	Total Amount
1	0.5% Au/TiO <sub>2</sub> -pH <sub>2</sub>	100	313	110	523
2	0.5% Au/TiO <sub>2</sub> -pO <sub>2</sub>	167	250	337	754
3	4% Au/TiO <sub>2</sub> -pH <sub>2</sub>	264	81	8	353
4	4% Au/TiO <sub>2</sub> -pO <sub>2</sub>	260	66	9	335
5	0.5% Au/Fe <sub>2</sub> O <sub>3</sub> /TiO <sub>2</sub> -pH <sub>2</sub>	86	114	41	241
6	0.5% Au/Fe <sub>2</sub> O <sub>3</sub> /TiO <sub>2</sub> -pO <sub>2</sub>	189	440	234	863
7	4% Au/Fe <sub>2</sub> O <sub>3</sub> /TiO <sub>2</sub> -pH <sub>2</sub>		298	54	352
8	4% Au/Fe <sub>2</sub> O <sub>3</sub> /TiO <sub>2</sub> -pO <sub>2</sub>	176	398	320	894
9	0.5% Au/MgO/TiO <sub>2</sub> -pH <sub>2</sub>	108	69	17	194
10	0.5% Au/MgO/TiO <sub>2</sub> -pO <sub>2</sub>	203	177	36	415
11	4% Au/MgO/TiO <sub>2</sub> -pH <sub>2</sub>		262	65	327
12	4% Au/MgO/TiO <sub>2</sub> -pO <sub>2</sub>		369	67	436

Table 5. Basic properties of catalysts.

Entry	Catalyst	Concentration of Basic Centers, $\mu\text{mol/g}$			
		Weak	Medium	Strong	Total Amount
1	0.5% Au/TiO <sub>2</sub> -pH <sub>2</sub>	46	66	15	127
2	0.5% Au/TiO <sub>2</sub> -pO <sub>2</sub>	56	20	13	89
3	4% Au/TiO <sub>2</sub> -pH <sub>2</sub>	15	41	17	73
4	4% Au/TiO <sub>2</sub> -pO <sub>2</sub>	34	29	21	84
5	0.5% Au/Fe <sub>2</sub> O <sub>3</sub> /TiO <sub>2</sub> -pH <sub>2</sub>	22	121	21	22
6	0.5% Au/Fe <sub>2</sub> O <sub>3</sub> /TiO <sub>2</sub> -pO <sub>2</sub>	37	91	47	175
7	4% Au/Fe <sub>2</sub> O <sub>3</sub> /TiO <sub>2</sub> -pH <sub>2</sub>	33	138	225	33
8	4% Au/Fe <sub>2</sub> O <sub>3</sub> /TiO <sub>2</sub> -pO <sub>2</sub>	20	74	30	124
9	0.5% Au/MgO/TiO <sub>2</sub> -pH <sub>2</sub>	23	163	32	23
10	0.5% Au/MgO/TiO <sub>2</sub> -pO <sub>2</sub>	44	38	26	108
11	4% Au/MgO/TiO <sub>2</sub> -pH <sub>2</sub>	23	78	69	23
12	4% Au/MgO/TiO <sub>2</sub> -pO <sub>2</sub>	51	41	21	113

As known, esterification of alcohols is catalyzed by H<sup>+</sup>. On the catalyst surface, most likely, the Brønsted acid centers act as the source of H<sup>+</sup>. At the same time, the formation of acid requires the presence of water, which on the catalyst surface can be in the form of pairs of Brønsted basic and acid centers (BBC and BAC), not excluding adsorbed water, which in turn, can dissociate on the catalyst surface with the formation of a pair of BBC and BAC. Accordingly, both acid and basic Brønsted centers must be present on the surface of the catalyst for the reaction to proceed along route A, including the esterification reaction (Scheme 1). In turn, BAC should mainly be on the surface of the catalyst for the reaction to proceed along route B.

In relation to the studied catalysts, a direct correlation between the acid-base properties determined by the TPD of NH<sub>3</sub> and CO<sub>2</sub> and the selectivity for acid or ester was not found (Table 6), which is most likely due to a combination of a number of reasons; namely, different activity of the catalysts, the presence of trivalent gold and metallic gold (due to the adsorption of the solvent on trivalent gold and metallic gold not only the deactivation of the catalyst occurs, but also a change in selectivity, which leads to disconformities between the acid-base properties and ester and/or acid selectivity), as well as some features of desorption methods for determining acid-base properties, namely TPD of NH<sub>3</sub> and CO<sub>2</sub>, described next.

Firstly, one should take into account the differences in temperatures: in this case, the oxidation of *n*-octanol tests (T = 80 °C), and the temperature ranges of the TPD study (CO<sub>2</sub> desorption starts from 25 °C, meanwhile NH<sub>3</sub> desorption starts from 100 °C to exclude the contribution of ammonia's physical adsorption). It should be noted also that mainly due to this reason, we take into account

only the concentrations of weak acid and basic centers. It is also well known that strong BAC and BBC are active participants in the catalytic process only at elevated temperatures (high-temperature gas-phase reactions).

**Table 6.** Acid-basic properties of catalysts and corresponding selectivity data in *n*-octanol oxidation.

Entry	Catalyst	Concentration of Weak Centers, $\mu\text{mol/g}$		Selectivity after 6 h, %		
		Basic	Acid	Ester	Acid	
1	0.5% Au/TiO <sub>2</sub> -H <sub>2</sub>		46	100	12	39
2	0.5% Au/TiO <sub>2</sub> -O <sub>2</sub>		56	167	20	52
3	4% Au/TiO <sub>2</sub> -H <sub>2</sub>		15	264	16	3
4	4% Au/TiO <sub>2</sub> -O <sub>2</sub>		34	260	42	3
5	0.5% Au/Fe <sub>2</sub> O <sub>3</sub> /TiO <sub>2</sub> -H <sub>2</sub>	22	121	86	17	29
6	0.5% Au/Fe <sub>2</sub> O <sub>3</sub> /TiO <sub>2</sub> -O <sub>2</sub>		37	189	43	21
7	4% Au/Fe <sub>2</sub> O <sub>3</sub> /TiO <sub>2</sub> -H <sub>2</sub>	33	138	298	42	0
8	4% Au/Fe <sub>2</sub> O <sub>3</sub> /TiO <sub>2</sub> -O <sub>2</sub>		20	176	51	1
9	0.5% Au/MgO/TiO <sub>2</sub> -H <sub>2</sub>	23	163	108	16	53
10	0.5% Au/MgO/TiO <sub>2</sub> -O <sub>2</sub>		44	203	42	20
11	4% Au/MgO/TiO <sub>2</sub> -H <sub>2</sub>	23	78	262	31	2
12	4% Au/MgO/TiO <sub>2</sub> -O <sub>2</sub>		51	369	42	0

Secondly, the probe molecules can change the chemical properties of the surface due to chemical transformations. Such examples are: ammonia dissociation at elevated temperatures on NH<sub>2</sub><sup>-</sup> and H<sup>+</sup>, giving false centers [69]; in addition, as shown in [70,71], a carbon dioxide molecule adsorbed on small gold nanoparticles can react with gold at room temperature (oxidizing metallic gold: 2Au<sup>0</sup> + CO<sub>2</sub> → Au<sup>+</sup>-O<sub>2</sub>-Au<sup>+</sup> + CO) and, accordingly, provide new basic sites, not directly related to the catalyst.

Thirdly, the probe molecules do not coincide in size with the reagent molecules and there will always be the issue of comparing the results of measuring acidity (basicity) and catalytic behavior.

Fourthly, the TPD methods of ammonia and CO<sub>2</sub> give information only about the strength and concentration of acid and basic centers, but not about their nature (Brønsted acid centers, Brønsted basic centers, Lewis acid centers and Lewis basic centers).

Nevertheless, for most of the studied systems, with the exception of samples with a high content of trivalent gold, there is a general tendency in the selectivity for acid and/or ester, depending on the acid-base properties of the catalysts (Table 6), namely:

For 0.5% Au/TiO<sub>2</sub>-H<sub>2</sub> and 0.5% Au/TiO<sub>2</sub>-O<sub>2</sub> samples (Table 6, Entries 1 and 2) with a content of weak acid (100 and 167  $\mu\text{mol/g}$ ) and basic (46 and 56  $\mu\text{mol/g}$ ) centers, with a ratio of 2:1 and 3:1, respectively, acid and ester were observed in the reaction products, with the predominant formation of acid (the reaction proceeds along route A, Scheme 1).

For samples 4% Au/TiO<sub>2</sub>-O<sub>2</sub>, 4% Au/Fe<sub>2</sub>O<sub>3</sub>/TiO<sub>2</sub>-pO<sub>2</sub>, 4% Au/MgO/TiO<sub>2</sub>-pO<sub>2</sub> and 4% Au/TiO<sub>2</sub>-pH<sub>2</sub> (Table 6, Entries 4, 8, 12 and 3 respectively), with a significant predominance of BAC compared to BBC, the acid formation does not exceed 3%, and we can assume that the reaction proceeds mainly along route B, taking into account the low conversion of *n*-octanol for these samples.

When comparing 0.5% Au/Fe<sub>2</sub>O<sub>3</sub>/TiO<sub>2</sub>-pO<sub>2</sub> and 0.5% Au/MgO/TiO<sub>2</sub>-pO<sub>2</sub> (Table 6, Entries 6 and 10) samples with a similar conversion level and roughly the same distribution of reaction products, we can also note that the concentrations of acidic and basic centers for these samples are close, the ratio of BAC/BBC = 4.6 and 5.1, respectively.

It should be noted that with an increase in the ratio of BAC/BBC, ester begins to prevail in the reaction products. This is clearly seen when comparing the corresponding values of BAC/BBC and the selectivity for ester and acid for samples 0.5% Au/TiO<sub>2</sub>-H<sub>2</sub> and 0.5% Au/TiO<sub>2</sub>-O<sub>2</sub> (BAC/BBC ≤ 3), 0.5% Au/Fe<sub>2</sub>O<sub>3</sub>/TiO<sub>2</sub>-pO<sub>2</sub> and 0.5% Au/MgO/TiO<sub>2</sub>-pO<sub>2</sub> (BAC/BBC > 4.5) and 4% Au/TiO<sub>2</sub>-O<sub>2</sub>, 4% Au/Fe<sub>2</sub>O<sub>3</sub>/TiO<sub>2</sub>-pO<sub>2</sub>, 4% Au/MgO/TiO<sub>2</sub>-pO<sub>2</sub> and 4% Au/TiO<sub>2</sub>-pH<sub>2</sub> (BAC/BBC > 7.5).

### 3.4. Quantum Chemical Simulation of *n*-Octanol Adsorption on Tetrahedral Gold Cluster

The optimized structures of octanol-Au<sub>20</sub> complexes with alcohol coordination on different gold atoms are shown in Figure 7. The energy changes during the formation of the complexes and the corresponding standard enthalpies are collected in Table 7. The optimization of octanol-Au<sub>20</sub> complex, in which alcohol is coordinated on the facet of the cluster, has led to the (C<sub>7</sub>H<sub>15</sub>CH<sub>2</sub>OH)Au<sub>20\_2</sub> complex with edge coordination. The OH group is involved in the interaction of the alcohol and the cluster. The calculated Au–O distances are 0.243 nm and 0.338 nm in (C<sub>7</sub>H<sub>15</sub>CH<sub>2</sub>OH)Au<sub>20\_1</sub> and (C<sub>7</sub>H<sub>15</sub>CH<sub>2</sub>OH)Au<sub>20\_2</sub>, respectively. According to the calculated data, the most favorable coordination of *n*-octanol on Au<sub>20</sub> is at the cluster's top. The binding energy of alcohol on the edge atoms is significantly lower.

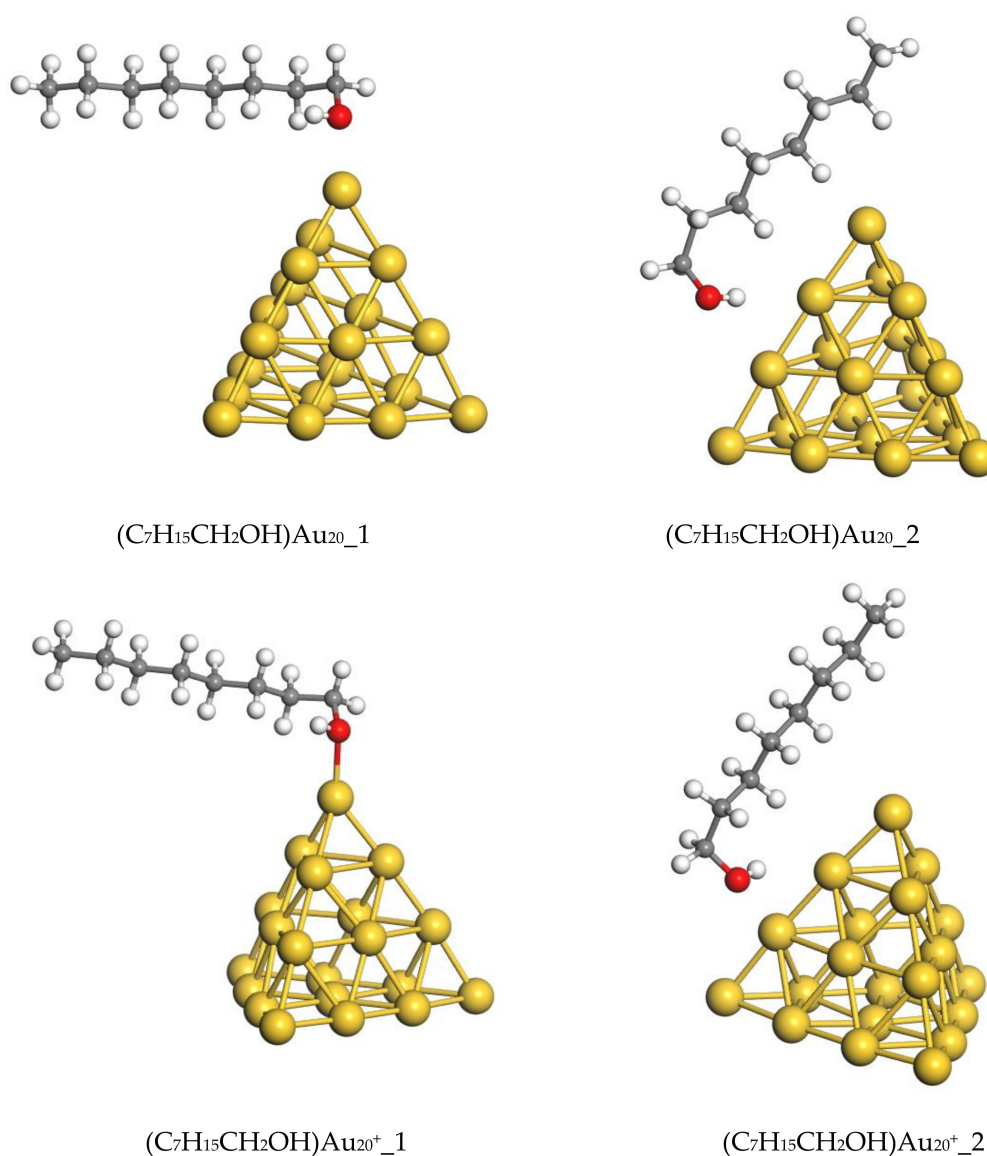


**Figure 7.** Optimized structures of *n*-octanol-Au<sub>20</sub> and *n*-octanol-Au<sub>20</sub><sup>+</sup> complexes.

Optimized structures of octanol-Au<sub>20</sub><sup>+</sup> have features similar to those of neutral octanol-Au<sub>20</sub>. In contrast, the calculated energy changes in Reaction (R2) (Table 7) are larger than in Reaction (R1). The binding energy of *n*-octanol with low-coordinated cationic gold atoms through OH-group is twice as much than that of low-coordinated gold atoms of neutral cluster. So, it can be concluded that the cationic sites play an important role in *n*-octanol activation on gold nanoparticles.

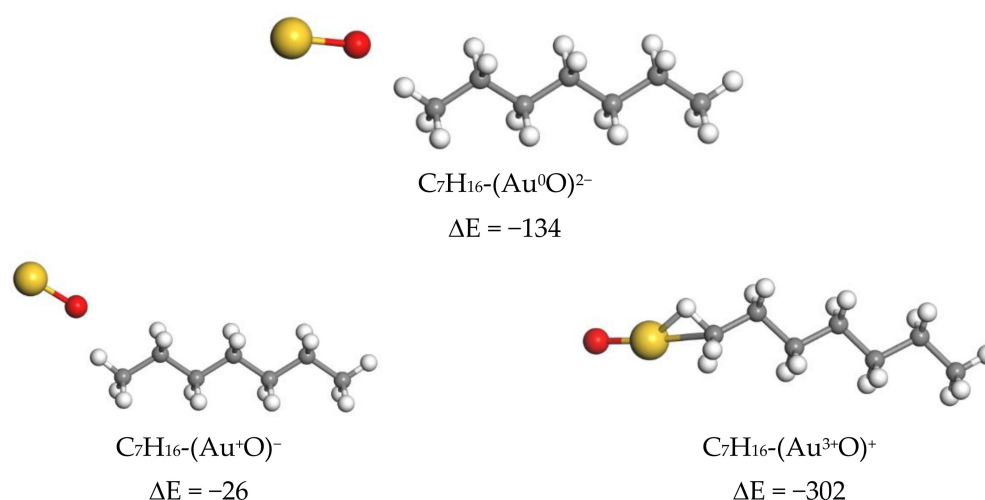
**Table 7.** Calculated energy change ( $\Delta E$  in kJ/mol) and standard enthalpy ( $\Delta H$ , kJ/mol) in the Reactions (R1) and (R2) of *n*-octanol with  $Au_{20}^z$  cluster ( $z = 0, +1$ ).

$z$	Complex	Type of Coordination	$\Delta E_1, \Delta E_2$	$\Delta H_1, \Delta H_2$
0	$(C_7H_{15}CH_2OH)Au_{20\_1}$	top	−40	−36
0	$(C_7H_{15}CH_2OH)Au_{20\_2}$	edge	−23	−20
+1	$(C_7H_{15}CH_2OH)Au_{20}^+_1$	top	−81	−78
+1	$(C_7H_{15}CH_2OH)Au_{20}^+_2$	edge	−55	−51

The adsorption of *n*-octanol on gold nanoparticles was simulated using DFT. It was shown that the low-coordinated gold atoms on the clusters top are the most active in the activation of alcohol. The binding energy of *n*-octanol with low-coordinated cationic gold atoms is sufficiently higher than on the neutral cluster. Based on the quantum chemistry, it can be concluded that the cationic sites play an important role in *n*-octanol adsorption.

### 3.5. Quantum Chemical Simulation of *n*-Heptane Adsorption on $Au^0$ , $Au^+$ and $Au^{3+}$

To reveal the role of  $Au^{3+}$  sites as inhibitors of the catalytic reaction, a quantum chemical simulation of the adsorption of the solvent (heptane) on simple models containing  $Au^0$ ,  $Au^+$  and  $Au^{3+}$  was performed.  $(Au^0O)^{2-}$ ,  $(Au^+O)^-$  and  $(Au^{3+}O)^+$  molecules were considered as models. Optimized structures of  $C_7H_{16}-(Au^0O)^{2-}$ ,  $C_7H_{16}-(Au^+O)^-$  and  $C_7H_{16}-(Au^{3+}O)^+$  complexes and calculated values of adsorption energies are presented in Figure 8.

**Figure 8.** Optimized structures of  $C_7H_{16}-(Au^0O)^{2-}$ ,  $C_7H_{16}-(Au^+O)^-$  and  $C_7H_{16}-(Au^{3+}O)^+$ . Calculated adsorption energies are given in kJ/mol.

Heptane can interact with  $(Au^0O)^{2-}$  with an adsorption energy of  $-134$  kJ/mol. This suggests that the  $Au^0$  sites may be partially occupied by solvent molecules. In contrast, heptane forms the most stable complex with  $(AuO)^+$ , in which gold is in the trivalent state. The calculated adsorption energy in  $C_7H_{16}-(Au^{3+}O)^+$  is  $-302$  kJ/mol. Using small models of active sites containing  $Au^0$ ,  $Au^+$  and  $Au^{3+}$ , it was shown that  $(Au^{3+}O)^+$  cations can strongly bind heptane.

## 4. Conclusions

The efficiency of gold catalysts supported on titania modified with iron or magnesium oxides and different gold contents (0.5 or 4 wt.%), and different thermal pretreatment conditions ( $H_2$  or  $O_2$ ), were investigated in the aerobic oxidation of *n*-octanol under mild conditions.

It was found that the catalytic behavior of  $Au/M_xO_y/TiO_2$  systems is primarily determined by the electronic state of the deposited gold; namely, the ratio between the  $Au^0$ ,  $Au^+$  and  $Au^{3+}$  states, which is

determined by the nature of the support and modifier, pretreatment conditions and gold concentration. A comparative study revealed that  $\text{Au}^+$  plays a decisive role in the oxidation of *n*-octanol and acts as an active site of  $\text{Au}/\text{M}_x\text{O}_y/\text{TiO}_2$  catalysts.  $\text{Au}^{3+}$  ions play an inhibitory role in the oxidation of *n*-octanol, due to the strong adsorption of the solvent and/or the blocking of highly charged trivalent gold ions by water molecules from the reaction. The low catalytic activity of the samples where only metallic gold was detected, according to the XPS and DRIFT CO data, was probably due to the partial blocking of the  $\text{Au}^0$  sites by the solvent that also led to inhibition of the oxidation of *n*-octanol, as in the case of  $\text{Au}^{3+}$ .

Density functional theory (DFT) simulations confirmed that  $\text{Au}^+$  sites play an important role, while  $\text{Au}^0$  and mostly  $\text{Au}^{3+}$  has an inhibitory effect *n*-octanol oxidation. By varying the nature of the modifier, the pretreatment atmosphere and the gold content, it was possible to obtain the optimal ratio between  $\text{Au}^0$ ,  $\text{Au}^+$  and  $\text{Au}^{3+}$  states, thereby increasing the efficiency of  $\text{Au}/\text{M}_x\text{O}_y/\text{TiO}_2$  catalysts in the oxidation of *n*-octanol.

It was found that reaction product distribution, notably, the formation of acid and/or ester, depends on the ratio of Brønsted acid centers to Brønsted basic centers: with a high ratio no acid is formed; with a low ratio of BAC/BBC selectivity to acid higher than to ester; intermediate values of BAC/BBC ratio produce mixture of acid and ester. It should be mentioned that, such a trend in dependence selectivity on BAC/BBC ratio was not observed only for three catalysts with a high content of trivalent gold, where mainly the adsorption of solvent occurs.

The best results of *n*-octanol oxidation were achieved using modified samples with the lower gold content after oxidizing pretreatment at 300 °C for 1 h, namely 0.5%  $\text{Au}/\text{MgO}/\text{TiO}_2$  and 0.5%  $\text{Au}/\text{Fe}_2\text{O}_3/\text{TiO}_2$ ; reaching 43% and 41% conversion after 6 h, with the highest selectivity to ester in both cases.

**Author Contributions:** E.P. carried out the catalysts preparation and pre-treatments, performed all catalytic tests, interpreted DRIFT CO data and wrote the first draft of the paper; E.K. and V.C.C. were responsible for the methodology of catalytic tests and supervised those experiments; E.K. interpreted XPS data and participated in the writing; Y.K. participated on the conceptualization and methodology of most characterization methods and carried out their corresponding pretreatments of catalysts; L.P. performed microscopy studies, elemental analysis and STEM data analysis; A.N.K. dealt with methodology of DRIFT CO technique and its implementation; D.G. was responsible for textural analysis and TPD methods and its interpretation; T.A.Z.P. and H.J.T.V. performed XRD and analyzed its results; M.H.F. was responsible for the XPS analyses; D.P. and N.N. performed DFT calculations and its interpretation; S.A.C.C., M.H.F., N.B., V.C.C., A.P. provided the means for the realization of this work and contributed to the supervision and paper revision. All authors have read and agreed to the published version of the manuscript.

**Funding:** This work was partially supported by the Associate Laboratory for Green Chemistry—LAQV, and financed by national funds from FCT/MCTES (UIDB/50006/2020)(Portugal), Tomsk Polytechnic University Competitiveness Enhancement Program, project VIU-RSCBMT-65/2019 and Russian Foundation of Basic Research, project 18-29-24037 (Russia), and MINECO project CTQ2017-86170-R (Spain).

**Acknowledgments:** The authors would like to thank David A. Domínguez for valuable technical support performing XPS measurements.

**Conflicts of Interest:** The authors declare no conflict of interest.

## References

1. Barati, B.; Moghadam, M.; Rahmati, A.; Mirkhani, V.; Tangestaninejad, S.; Mohammadpoor-Baltork, I. Direct oxidation of alcohols to carboxylic acids over ruthenium hydride catalyst with diphenylsulfoxide oxidant. *Inorg. Chem. Commun.* **2013**, *29*, 114–117. [[CrossRef](#)]
2. Corberán, V.C.; González-Pérez, M.E.; Martínez-González, S.; Gómez-Avilés, A. Green oxidation of fatty alcohols: Challenges and opportunities. *Appl. Catal. A-Gen.* **2014**, *474*, 211–223. [[CrossRef](#)]
3. Tojo, G.; Fernández, M. *Oxidation of Primary Alcohols to Carboxylic Acids: A Guide to Current Common Practice*; Springer: Berlin, Germany, 2006.
4. Zhao, M.; Li, J.; Song, Z.; Desmond, R.; Tschaen, D.M.; Grabowski, E.J.J.; Reider, P.J. A novel chromium trioxide catalyzed oxidation of primary alcohols to the carboxylic acids. *Tetrahedron Lett.* **1998**, *39*, 5323–5326. [[CrossRef](#)]
5. Augustine, R.L. *Heterogeneous Catalysis for The Synthetic Chemist*; Dekker: New York, NY, USA, 1996.

6. Sheldon, R.A. Catalysis: The key to waste minimization. *J. Chem. Tech. Biotechnol.* **1997**, *68*, 381–388. [CrossRef]
7. Schmieder-van de Vondervoort, L.; Bouttemy, S.; Padron, J.M.; Le Bras, J.; Muzart, J.; Alsters, P.L. Chromium catalyzed oxidation of (homo)allylic and (homo)propargylic alcohols with sodium periodate to ketones or carboxylic acids. *Synlett* **2002**, *2*, 243–246. [CrossRef]
8. Sheldon, R.A.; Arends, I.W.C.E.; Dijkstra, A. New developments in catalytic alcohol oxidation for fine chemicals synthesis. *Catal. Today* **2000**, *57*, 157–166. [CrossRef]
9. Werpy, T.; Petersen, G. *Top Value Added Chemicals from Biomass: Volume I—Results of Screening for Potential Candidates from Sugars and Synthesis Gas*; U. S. Department of Energy: Oak Ridge, CO, USA, 2004.
10. Mori, K.; Yamaguchi, K.; Hara, T.; Mizugaki, T.; Ebitani, K.; Kaneda, K. Controlled synthesis of hydroxyl apatite-supported palladium complexes as highly efficient heterogeneous catalysts. *J. Am. Chem. Soc.* **2002**, *124*, 11572–11573. [CrossRef]
11. Nishimura, T.; Onoue, T.; Ohe, K.; Uemura, S. Palladium(II)-catalyzed oxidation of alcohols to aldehydes and ketones by molecular oxygen. *J. Org. Chem.* **1999**, *64*, 6750–6755. [CrossRef]
12. Hasan, M.; Musawir, M.; Davey, P.N.; Kozhevnikov, I.V. Oxidation of primary alcohols to aldehydes with oxygen catalyzed by tetra-npropylammoniumperuthenate. *J. Mol. Catal. A-Chem.* **2002**, *180*, 77–84. [CrossRef]
13. Yamaguchi, K.; Mori, K.; Mizugaki, T.; Ebitani, K.; Kaneda, K. Creation of a monomeric Ru species on the surface of hydroxyapatite as an efficient heterogeneous catalyst for aerobic alcohol oxidation. *J. Am. Chem. Soc.* **2000**, *122*, 7144–7145. [CrossRef]
14. Wang, H.; Fan, W.; He, Y.; Wang, J.; Kondo, J.N.; Tatsumi, T. Selective oxidation of alcohols to aldehydes/ketones over copper oxide-supported gold catalysts. *J. Catal.* **2013**, *299*, 10–19. [CrossRef]
15. Hashmi, A.S.K.; Lothschutz, C.; Ackermann, M.; Doepp, R.; Anantharaman, S.; Marchetti, B.; Bertagnolli, H.; Rominger, F. Gold Catalysis: In situ EXAFS study of homogeneous oxidative esterification. *Chem. Eur. J.* **2010**, *16*, 8012–8019. [CrossRef] [PubMed]
16. Enache, D.I.; Edwards, J.K.; Landon, P.; Solsona-Espriu, B.; Carley, A.F.; Herzing, A.A.; Watanabe, M. Solvent-free oxidation of primary alcohols to aldehydes using Au-Pd/TiO<sub>2</sub> catalysts. *Science* **2006**, *311*, 362–365. [CrossRef] [PubMed]
17. Martins, L.M.D.R.S.; Carabineiro, S.A.C.; Wang, J.; Rocha, B.G.M.; Maldonado-Hodar, F.J.; Latourrette de Oliveira Pombeiro, A.J. Supported gold nanoparticles as reusable catalysts for oxidation reactions of industrial significance. *ChemCatChem* **2017**, *9*, 1211–1221. [CrossRef]
18. Kohlpaintner, C.; Schulte, M.; Falbe, J.; Lappe, P.; Weber, J.; Frey, G.D. Aldehydes, Aliphatic. In *Ullmann's Encyclopedia of Industrial Chemistry*; Wiley-VCH Verlag GmbH: Weinheim, Germany, 2013.
19. Beare-Rogers, J.; Dieffenbacher, A.; Holm, J.V. Lexicon of lipid nutrition (IUPAC Technical Report). *Pure Appl. Chem.* **2001**, *73*, 685–744. [CrossRef]
20. Harrigan-Farrelly, J. Caprylic (Octanoic) Acid registration review final decision. *Federal Register*. **2009**, *74*, 30080–30081.
21. Voller, B.; Lines, E.; McCrossin, G.; Tinaz, S.; Lungu, C.; Grimes, G.; Starling, J.; Potti, G.; Buchwald, P. Dose-escalation study of octanoic acid in patients with essential tremor. *J. Clin. Invest.* **2016**, *126*, 1451–1457. [CrossRef]
22. Lowell, S.Y.; Kelley, R.T.; Monahan, M.; Hosbach-Cannon, C.J.; Colton, R.H.; Mihaila, D. The effect of octanoic acid on essential voice tremor: A Double-Blind, Placebo-Controlled Study. *Laryngoscope* **2018**, *129*, 1882–1890. [CrossRef]
23. PubChem. “Octanoic acid”. Available online: <https://pubchem.ncbi.nlm.nih.gov/compound/379> (accessed on 20 March 2020).
24. Li, W.; Wang, A.; Liu, X.; Zhang, T. Silica-supported Au–Cu alloy nanoparticles as an efficient catalyst for selective oxidation of alcohols. *Appl. Catal. A-Gen.* **2012**, *433–434*, 146–151. [CrossRef]
25. Su, F.-Z.; Chen, M.; Wang, L.-C.; Huang, X.-S.; Liu, Y.-M.; Cao, Y.; He, H.-Y.; Fan, K.-N. Aerobic oxidation of alcohols catalyzed by gold nanoparticles supported on gallia polymorphs. *Catal. Commun.* **2008**, *9*, 1027–1032. [CrossRef]
26. Liu, H.; Liu, Y.; Li, Y.; Tang, Z.; Jiang, H. Metal-organic framework supported gold nanoparticles as a highly active heterogeneous catalyst for aerobic oxidation of alcohols. *J. Phys. Chem. C* **2010**, *114*, 13362–13369. [CrossRef]

27. Haider, P.; Baiker, A. Gold supported on Cu–Mg–Al-mixed oxides: Strong enhancement of activity in aerobic alcohol oxidation by concerted effect of copper and magnesium. *J. Catal.* **2007**, *248*, 175–187. [[CrossRef](#)]
28. Kaskow, I.; Sobczak, I.; Ziolk, M.; Corberan, V.C. The effect of support properties on *n*-octanol oxidation performed on gold–silver catalysts supported on MgO, ZnO and Nb<sub>2</sub>O<sub>5</sub>. *J. Mol. Catal.* **2020**, *482*, 110674. [[CrossRef](#)]
29. Kotolevich, Y.; Kolobova, E.; Khramov, E.; Farias, M.H.; Zubavichus, Y.; Tiznado, H.; González-Pérez, M.E.; Corberán, V.C.; Mota-Morales, J.D.; Pestryakov, A.N.; et al. *n*-Octanol oxidation on Au/TiO<sub>2</sub> catalysts promoted with La and Ce oxides. *J. Mol. Catal.* **2017**, *427*, 1–10. [[CrossRef](#)]
30. Kotolevich, Y.; Kolobova, E.; Mamontov, G.; Khramov, E.; Cabrera Ortega, J.E.; Tiznado, H.; Farias, M.H.; Bogdanchikova, N.; Zubavichus, Y.V.; Mota-Morales, J.D.; et al. Au/TiO<sub>2</sub> catalysts promoted with Fe and Mg for *n*-octanol oxidation under mild conditions. *Catal. Today* **2016**, *278*, 104–112. [[CrossRef](#)]
31. Kolobova, E.; Pakrieva, E.; Pascual, L.; Cortés Corberán, V.; Bogdanchikova, N.; Farias, M.; Pestryakov, A. Selective oxidation of *n*-octanol on unmodified and La-modified nanogold catalysts: Effect of metal content. *Catal. Today* **2019**, *333C*, 127–132. [[CrossRef](#)]
32. Pakrieva, E.; Kolobova, E.; Mamontov, G.; Bogdanchikova, N.; Farias, M.H.; Pascual, L.; Cortés Corberán, V.; Martínez González, S.; Carabineiro, S.A.C.; Pestryakov, A. Green oxidation of *n*-octanol on supported nanogold catalysts: Formation of gold active sites under combined effect of gold content, additive nature and redox pretreatment. *ChemCatChem* **2019**, *11*, 1615–1624. [[CrossRef](#)]
33. Pakrieva, E.; Ribeiro, A.P.C.; Kolobova, E.; Martins, L.M.D.R.S.; Carabineiro, S.A.C.; German, D.; Pichugina, D.; Jiang, C.; Pombeiro, A.J.L.; Bogdanchikova, N.; et al. Supported gold nanoparticles as catalysts in peroxidative and aerobic oxidation of 1-phenylethanol under mild conditions. *Nanomaterials* **2020**, *10*, 151. [[CrossRef](#)]
34. Zanella, R.; Giorgio, S.; Henry, C.R.; Louis, C. Alternative methods for the preparation of gold nanoparticles supported on TiO<sub>2</sub>. *J. Phys. Chem. B* **2002**, *106*, 7634–7642. [[CrossRef](#)]
35. Zanella, R.; Louis, C. Influence of the conditions of thermal treatments and of storage on the size of the gold particles in Au/TiO<sub>2</sub> samples. *Catal. Today* **2005**, *107–108*, 768–777. [[CrossRef](#)]
36. Perdew, J.P.; Burke, K.; Ernzerhof, M. Generalized Gradient Approximation Made Simple. *Phys. Rev. Lett.* **1996**, *77*, 3865–3868. [[CrossRef](#)] [[PubMed](#)]
37. Xiao, L.; Tollberg, B.; Hu, X.; Wang, L. Structural study of gold clusters. *J. Chem. Phys.* **2006**, *124*, 114309. [[CrossRef](#)] [[PubMed](#)]
38. Mukhamedzyanova, D.F.; Ratmanova, N.K.; Pichugina, D.A.; Kuzmenko, E.N. A structural and stability evaluation of Au<sub>12</sub> from an isolated cluster to the deposited material. *J. Phys. Chem. C* **2012**, *116*, 11507–11518. [[CrossRef](#)]
39. Beletskaya, A.V.; Pichugina, D.A.; Shestakov, A.F.; Kuz'menko, N.E. Formation of H<sub>2</sub>O<sub>2</sub> on Au<sub>20</sub> and Au<sub>19</sub>Pd clusters: Understanding the structure effect on the atomic level. *J. Phys. Chem. A* **2013**, *117*, 6817–6826. [[CrossRef](#)]
40. Laikov, D.N.; Ustynyuk, Y.A. PRIRODA-04: A Quantum-Chemical Program Suite. New possibilities in the study of molecular systems with the application of parallel computing. *Russ. Chem. Bull.* **2005**, *54*, 820–826. [[CrossRef](#)]
41. Sadovnichy, V.; Tikhonravov, A.; Voevodin, V.; Opanasenko, V. *Contemporary High Performance Computing: From Petascale Toward Exascale*; CRC Press, Chapman & Hall/CRC Computational Science: Boca Raton, FL, USA, 2013; pp. 283–307.
42. Kolobova, E.; Kotolevich, Y.; Pakrieva, E.G.; Mamontov, G.; Farias, M.H.; Bogdanchikova, N.; Pestryakov, A. Causes of activation and deactivation of modified nanogold catalysts during prolonged storage and redox treatments. *Molecules* **2016**, *21*, 486. [[CrossRef](#)]
43. Ishida, T.; Ogihara, Y.; Ohashi, H.; Akita, T.; Honma, T.; Oji, H.; Haruta, M. Base-free direct oxidation of 1-octanol to octanoic acid and its octyl ester over supported gold catalysts. *ChemSusChem* **2012**, *5*, 2243–2248. [[CrossRef](#)]
44. Carabineiro, S.A.C.; Bogdanchikova, N.; Avalos-Borja, M.; Pestryakov, A.; Tavares, P.B.; Figueiredo, J.L. Gold supported on metal oxides for carbon monoxide oxidation. *Nano Res.* **2011**, *4*, 180–193. [[CrossRef](#)]
45. Furusawa, T.; Seshan, K.; Lercher, J.A.; Lefferts, L.; Aika, K. Selective reduction of NO to N<sub>2</sub> in the presence of oxygen over supported silver catalysts. *Appl. Catal. B-Environ.* **2002**, *37*, 205–216. [[CrossRef](#)]
46. Herzing, A.A.; Kiely, C.J.; Carley, A.F.; Landon, P.; Hutchings, G.J. Identification of active gold nanoclusters on iron oxide supports for CO oxidation. *Science* **2008**, *321*, 1331–1335. [[CrossRef](#)]



47. Chrétien, S.; Buratto, S.K.; Metiu, H. Catalysis by very small Au clusters. *Curr. Opin. Solid State Mater. Sci.* **2007**, *11*, 62–75. [[CrossRef](#)]
48. Moulder, J.F.; Stickle, W.F.; Sobol, P.E.; Bomben, K.D. *Handbook of X-Ray Photoelectron Spectroscopy*; Chastain, J., Ed.; Perkin-Elmer Corporation: Eden Prairie, MN, USA, 1992.
49. Casaletto, M.P.; Longo, A.; Martorana, A.; Prestianni, A.; Venezia, A.M. XPS study of supported gold catalysts: The role of Au<sup>0</sup> and Au<sup>+δ</sup> species as active sites. *Surf. Interface Anal.* **2006**, *38*, 215–218. [[CrossRef](#)]
50. Costa, V.V.; Estrada, M.; Demidova, Y.; Prosvirin, I.; Kriventsov, V.; Cotta, R.F.; Fuentes, S.; Simakov, A.; Gusevskaya, E. Gold nanoparticles supported on magnesium oxide as catalysts for the aerobic oxidation of alcohols under alkali-free conditions. *J. Catal.* **2012**, *292*, 148–156. [[CrossRef](#)]
51. Feng, R.; Li, M.; Liu, J. Synthesis of core-shell Au@Pt nanoparticles supported on Vulcan XC-72 carbon and their electrocatalytic activities for methanol oxidation. *Colloids Surf. A* **2012**, *406*, 6–12. [[CrossRef](#)]
52. Zhang, Y.L.; Xiao, Q.; Bao, Y.S.; Zhang, Y.J.; Bottle, S.; Sarina, S.; Zhaorigetu, B.; Zhu, H.Y. Direct photocatalytic conversion of aldehydes to esters using supported gold nanoparticles under visible light irradiation at room temperature. *J. Phys. Chem. C* **2014**, *118*, 19062–19069. [[CrossRef](#)]
53. Pojanavaraphan, C.; Satitthai, U.; Luengnaruemitchai, A.; Gulari, E. Activity and stability of Au/CeO<sub>2</sub>-Fe<sub>2</sub>O<sub>3</sub> catalysts for the hydrogen production via oxidative steam reforming of methanol. *J. Ind. Eng. Chem.* **2015**, *22*, 41–52. [[CrossRef](#)]
54. Epling, W.S.; Hoflund, G.B.; Weaver, J.F.; Tsubota, S.; Haruta, M. Surface characterization study of Au/α-Fe<sub>2</sub>O<sub>3</sub> and Au/Co<sub>3</sub>O<sub>4</sub> low-temperature CO oxidation catalysts. *J. Phys. Chem.* **1996**, *100*, 9929–9934. [[CrossRef](#)]
55. Luengnaruemitchai, A.; Srihamat, K.; Pojanavaraphan, C.; Wanchanthuek, R. Activity of Au/Fe<sub>2</sub>O<sub>3</sub>-TiO<sub>2</sub> catalyst for preferential CO oxidation. *Int. J. Hydrog. Energy* **2015**, *40*, 13443–13455. [[CrossRef](#)]
56. Penkova, A.; Chakarova, K.; Laguna, O.H.; Hadjiivanov, K.; Romero Saria, F.; Centeno, M.A.; Odriozola, J.A. Redox chemistry of gold in a Au/FeOx/CeO<sub>2</sub> CO oxidation catalyst. *Catal. Commun.* **2009**, *10*, 1196–1202. [[CrossRef](#)]
57. Pestryakov, A.N.; Davydov, A.A. Active electronic states of silver catalysts for methanol selective oxidation. *Appl. Catal. A-Gen.* **1994**, *120*, 7–15. [[CrossRef](#)]
58. Simakov, A.; Tuzovskaya, I.; Pestryakov, A.; Bogdanchikova, N.; Gurin, V.; Avalos, M.; Fariás, M.H. On the nature of active gold species in zeolites in CO oxidation. *Appl. Catal. A-Gen.* **2007**, *331*, 121–128. [[CrossRef](#)]
59. Bogdanchikova, N.; Pestryakov, A.; Tuzovskaya, I.; Zepeda, T.A.; Farias, M.H.; Tiznado, H.; Martynyuk, O.A. Effect of redox treatments on activation and deactivation of gold nanospecies supported on mesoporous silica in CO oxidation. *Fuel* **2013**, *110*, 40–47. [[CrossRef](#)]
60. Minico, S.; Scire, S.; Crisafalli, C.; Visco, A.M.; Galvagno, S. FT-IR study of Au/Fe<sub>2</sub>O<sub>3</sub> catalysts for CO oxidation at low temperature. *Catal. Lett.* **1997**, *47*, 273–276. [[CrossRef](#)]
61. Hadjiivanov, K.I.; Vayssilov, G.N. Characterization of oxide surfaces and zeolites by carbon monoxide as an IR probe molecule. *Adv. Catal.* **2002**, *47*, 307–511.
62. Qiu, S.; Ohnishi, R.; Ichikawa, M. Novel preparation of gold(I) carbonyls and nitrosyls in NaY zeolite and their catalytic activity for NO reduction with CO. *J. Chem. Soc. Chem. Commun.* **1992**, 1425–1427. [[CrossRef](#)]
63. Mihaylov, M.; Knoezinger, H.; Hadjiivanov, K.; Gates, B.C. Characterization of the oxidation states of supported gold species by IR spectroscopy of adsorbed CO. *Chem. Ing. Tech.* **2007**, *79*, 795–806. [[CrossRef](#)]
64. Chen, Y.-W.; Chen, H.-J.; Lee, D.-S. Au/Co<sub>3</sub>O<sub>4</sub>-TiO<sub>2</sub> catalysts for preferential oxidation of CO in H<sub>2</sub> stream. *J. Mol. Catal. A-Chem.* **2012**, *363–364*, 470–480. [[CrossRef](#)]
65. Eblagon, K.M.; Pastrana-Martinez, L.M.; Pereira, M.F.R.; Figueiredo, J.L. Cascade conversion of cellobiose to gluconic acid: The large impact of the small modification of electronic interaction on the performance of Au/TiO<sub>2</sub> bifunctional catalysts. *Energy Technol.* **2018**, *6*, 1675–1686. [[CrossRef](#)]
66. Ganduglia-Pirovano, M.V.; Hofmann, A.; Sauer, J. Oxygen vacancies in transition metal and rare earth oxides: Current state of understanding and remaining challenges. *Surf. Sci. Rep.* **2007**, *62*, 219–270. [[CrossRef](#)]
67. Ariyanti, D.; Mills, L.; Dong, J.; Yao, Y.; Gao, W. NaBH<sub>4</sub> modified TiO<sub>2</sub>: Defect site enhancement related to its photocatalytic activity. *Mater. Chem. Phys.* **2017**, *199*, 571–576. [[CrossRef](#)]
68. Liu, H.; Ma, H.T.; Li, X.Z.; Li, W.Z.; Wu, M.; Bao, X.H. The enhancement of TiO<sub>2</sub> photocatalytic activity by hydrogen thermal treatment. *Chemosphere* **2003**, *50*, 39–46. [[CrossRef](#)]
69. Glazneva, T.S.; Kotsarenko, N.S.; Paukshtis, E.A. Surface acidity and basicity of oxide catalysts: From aqueous suspensions to in situ measurements. *Kinet. Catal.* **2008**, *49*, 859–867. [[CrossRef](#)]

70. Mihaylov, M.; Ivanova, E.; Hao, Y.; Hadjiivanov, K.; Gates, B.C.; Knozinger, H. Oxidation by CO<sub>2</sub> of Au<sup>0</sup> species on La<sub>2</sub>O<sub>3</sub>-supported gold clusters. *Chem. Commun.* **2008**, 175–177. [[CrossRef](#)] [[PubMed](#)]
71. Mihaylov, M.; Ivanova, E.; Hao, Y.; Hadjiivanov, K.; Knozinger, H.; Gates, B.C. Gold supported on La<sub>2</sub>O<sub>3</sub>: Structure and reactivity with CO<sub>2</sub> and implications for CO oxidation catalysis. *J. Phys. Chem. C* **2008**, *112*, 18973–18983. [[CrossRef](#)]



© 2020 by the authors. Licensee MDPI, Basel, Switzerland. This article is an open access article distributed under the terms and conditions of the Creative Commons Attribution (CC BY) license (<http://creativecommons.org/licenses/by/4.0/>).